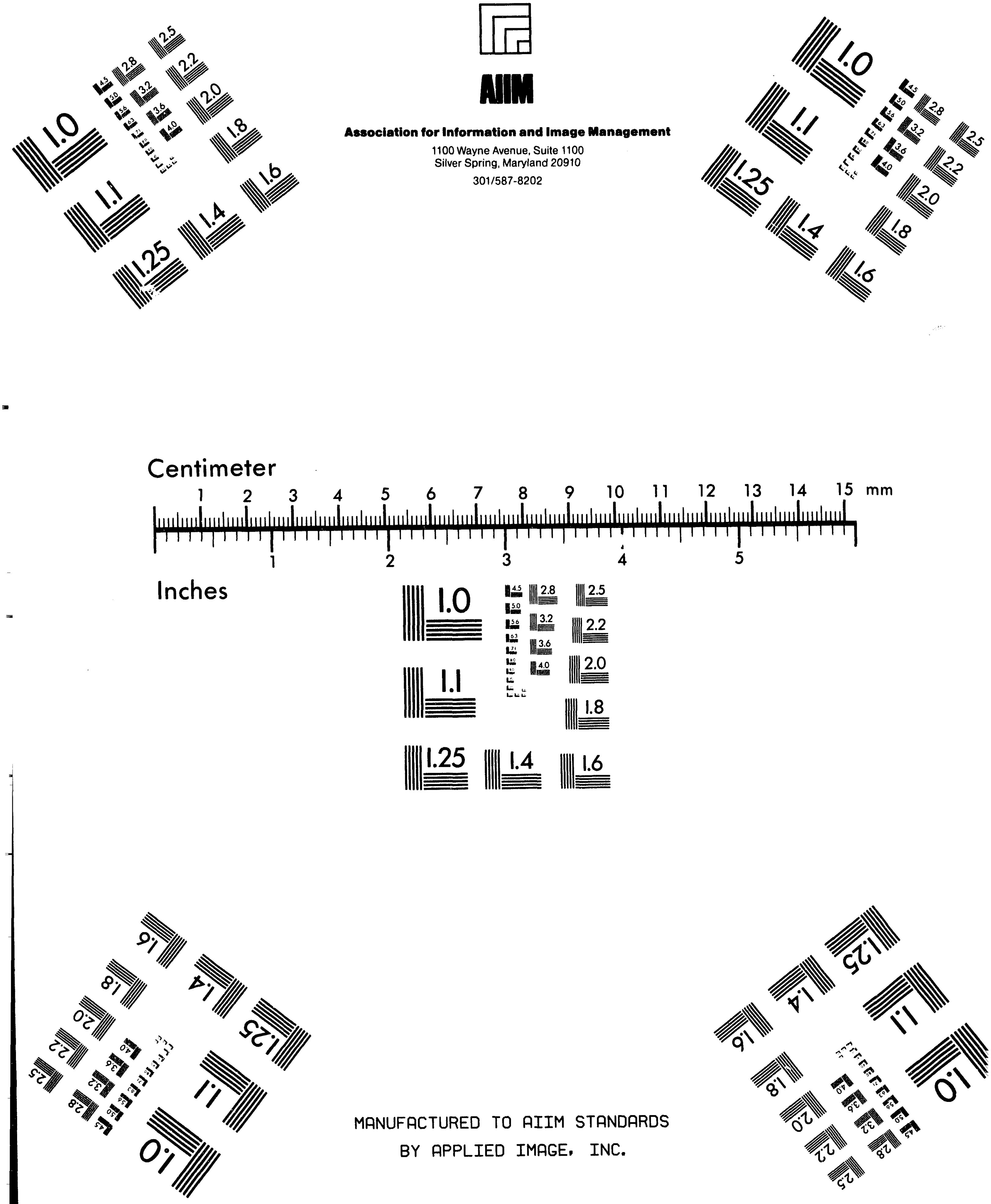

SAND92-0847
Unlimited Release
Printed July 1994

Distribution
Category UC-814

The Effect of Frequency on Young's Modulus and Seismic Wave Attenuation

R. H. Price
YMP Performance Assessment Applications Department
Sandia National Laboratories
Albuquerque, NM 87185

R. J. Martin, III and R. W. Haupt
New England Research, Inc.
White River Junction, VT 05001

ABSTRACT

Laboratory experiments were performed to measure the effect of frequency, water-saturation, and strain amplitude on Young's modulus and seismic wave attenuation on rock cores recovered on or near the site of a potential nuclear waste repository at Yucca Mountain, Nevada. The purpose of this investigation is to perform the measurements using four techniques: cyclic loading, waveform inversion, resonant bar, and ultrasonic velocity. The measurements ranged in frequency between 10^{-2} and 10^{6} Hz.

For the dry specimens Young's modulus and attenuation were independent of frequency; that is, all four techniques yielded nearly the same values for modulus and attenuation. For saturated specimens, a frequency dependence for both Young's modulus and attenuation was observed. In general, saturation reduced Young's modulus and increased seismic wave attenuation. The effect of strain amplitude on Young's modulus and attenuation was measured using the cyclic loading technique at a frequency of 10^{-1} Hz. The effect of strain amplitude in all cases was small. For some rocks, such as the potential repository horizon of the Topopah Spring Member tuff (TSw2), the effect of strain amplitude on both attenuation and modulus was minimal.

This report was prepared under the Yucca Mountain Project WBS number 1.2.3.2.7.1.3.
The data in this report was developed subject to QA controls in QAGR S1232713; the data is not qualified and is not to be used for licensing.

CONTENTS

List of Figures

List of Tables

1.0 INTRODUCTION

In light of the requirements for reliable input parameters into the rheological models for the potential nuclear waste repository at Yucca Mountain, a suite of measurements was carried out to study the effects of frequency, water saturation, and excitation strain amplitude on the elastic moduli and seismic wave attenuation on tuff. In most previous studies, only one measurement technique over a limited frequency band was employed. Therefore, to understand the complete frequency dependence for a specific rock, data on that rock from diverse sources were pieced together. The approach here was to use multiple techniques on the same rock core to determine Young's modulus, E, and extensional wave attenuation, Q_E^{-1}, as a function of frequency, water saturation, and strain amplitude.

Seismic attenuation contributes significantly to the amplitudes and spectra of ground motion measured at the surface. Attenuation is greatest in soils (unconsolidated sediments); less, but significant, in consolidated sediments. Even at hard, crystalline rock sites, attenuation takes place mostly in the upper few kilometers of the crust (Toksöz et al., 1990). This is due primarily to physical mechanisms responsible for attenuation.

The three most important mechanisms for seismic attenuation are: (1) relative motions and the resulting friction across grain boundaries, microfractures, and between zones with different mechanical properties; (2) motions of fluids, such as water, induced by seismic waves; and (3) scattering of waves by the heterogeneity (i.e., mechanical properties contrasts) in rocks. Friction is the single most important mechanism for seismic attenuation at shallow depths. Because of low confining pressure and large surface areas that are not bound strongly, seismic waves easily cause motions and loss of energy due to friction (Walsh, 1969; Mavko and Nur, 1979; and Toksöz and Johnston, 1981). At greater depths the grains are bound more strongly due to overburden pressure, compaction, and lithification. Relative motions between grains induced by the waves decrease, with a resulting decrease in attenuation.

The attenuation properties in rocks and soils are specified by a wide range of measures in seismology and engineering. In order to avoid confusion, it is important to present a brief definition of terms that are used and to show how they relate to each other. The most commonly used measures of attenuation are: attenuation coefficient, α; quality factor, Q; and its inverse, Q^{-1}, commonly referred to as attenuation; logarithmic decrement, δ; loss tangent, tan ϕ; and damping coefficient, D. Leaving out small second-order corrections proportional to α^2, the above parameters are related by

$$\frac{1}{Q} = \frac{\alpha V}{\pi f} = \frac{\delta}{\pi} = \tan\phi = 2D = \frac{\Delta\varepsilon}{2\pi\varepsilon} \quad (1)$$

where V is wave velocity, f is frequency, $\Delta\varepsilon$ is the energy loss per cycle and ε is the strain energy stored in the specimen during a cycle (Toksöz and Johnston, 1981).

Significant differences in elastic moduli and wave attenuation have been observed for rocks measured with different laboratory and field techniques. These differences can be attributed to the frequency and strain amplitude dependencies in the anelastic response of rock to loading. Anelastic mechanisms in rock produce a phase lag between stress and strain and affect the measured moduli and attenuation. The modulus, M, is represented by a complex quantity,

$$M = M_R + iM_I \quad (2)$$

where M_R and M_I are the real and imaginary parts of the modulus, respectively. The phase lag, ϕ, is a direct measure of the intrinsic loss or attenuation, Q^{-1} (Toksöz and Johnston, 1981),

$$Q^{-1} = M_I / M_R = \tan\phi \quad (3)$$

Previous studies have reported frequency, strain amplitude, and saturation dependencies on elastic moduli and Q^{-1} in many types of crustal rocks (Gordon and Davis, 1968; Toksöz et al., 1979; Winkler et al., 1979; Spencer, 1981; Dunn, 1986; Paffenholz and Burkhardt, 1989). A variety of laboratory techniques were used for these measurements; the method used depends on the frequency of interest. Other factors such as rock porosity, pore geometry, and pore fluid pressure also influence the elastic and anelastic rock properties.

Spencer (1981) used a cyclic loading technique to examine the effect of frequency and fluid saturation on the modulus and attenuation for Spergen Limestone, Navajo Sandstone, and Oklahoma Granite. For dry rocks, the modulus and attenuation were independent of frequency. When the specimens were saturated with water, the modulus decreased and a frequency dependence was observed. For example at 10Hz, Young's modulus of the sandstone, decreased by 56% due to saturation. There was a small increase in modulus with increasing frequency between 10 and 5×10^2 Hz. Attenuation was significantly greater for water-saturated rocks than for the dry state at all frequencies.

Tittmann et al. (1980) and Bulau et al. (1984) used a resonant bar technique to measure modulus and Q^{-1} as a function of water saturation at frequencies between 10^3 and 10^4 Hz for a wide variety of rocks. In general, the attenuation increased and the modulus decreased as the water saturation increased.

Attenuation and elastic moduli at ultrasonic frequencies have been reported by several investigators (e.g. Toksöz et al., 1979; Coyner, 1984). These data show that Young's modulus is typically greater for water-saturated rocks than for dry rocks. Furthermore, the attenuation in dry rocks is greater than that for saturated rocks.

Strain amplitude has also been shown to affect Young's modulus and Q^{-1} in granite and sandstone. With increasing strain amplitude, above 10^{-7} or so, Young's modulus decreases and Q^{-1} increases (Winkler et al., 1979; Johnston and Toksöz, 1981; Bulau et al., 1984). The increase is more pronounced at higher strain amplitudes. The effect has been observed for both dry and saturated conditions.

2.0 EXPERIMENTAL PROCEDURE

Young's modulus and extensional attenuation have been determined as functions of frequency, strain amplitude, and water saturation for eleven tuff samples recovered from boreholes and an outcrop on or near Yucca Mountain, Nevada. A map showing the location of the boreholes on Yucca Mountain is given in Figure 1. The geological stratigraphy for the tuffs at Yucca Mountain is presented in Figure 2. Oritz et al (1985) proposed a thermal/mechanical stratigraphy based on the physical properties of the tuffs. A correlation between the thermal/mechanical units and the geological stratigraphy is also shown in Figure 2.

The samples recovered from the boreholes and prepared for testing in this study are listed in Table 1. Four techniques were used to cover frequencies ranging from 10^{-2} to 10^6 Hz. The strain amplitude dependence was measured at a single frequency, using a cyclic loading technique. Stress-strain hysteresis loops were generated at 0.1 Hz with peak strain amplitudes that ranged from 10^{-7} to 10^{-4}. The methods along with the corresponding sample size are given in Table 2.

The measurements were carried out under room-dry and fully water-saturated conditions. The sequence of measurements began with the cyclic loading experiments. The samples were then subdivided into smaller specimens for the waveform inversion, resonant bar, and ultrasonic velocity measurements.

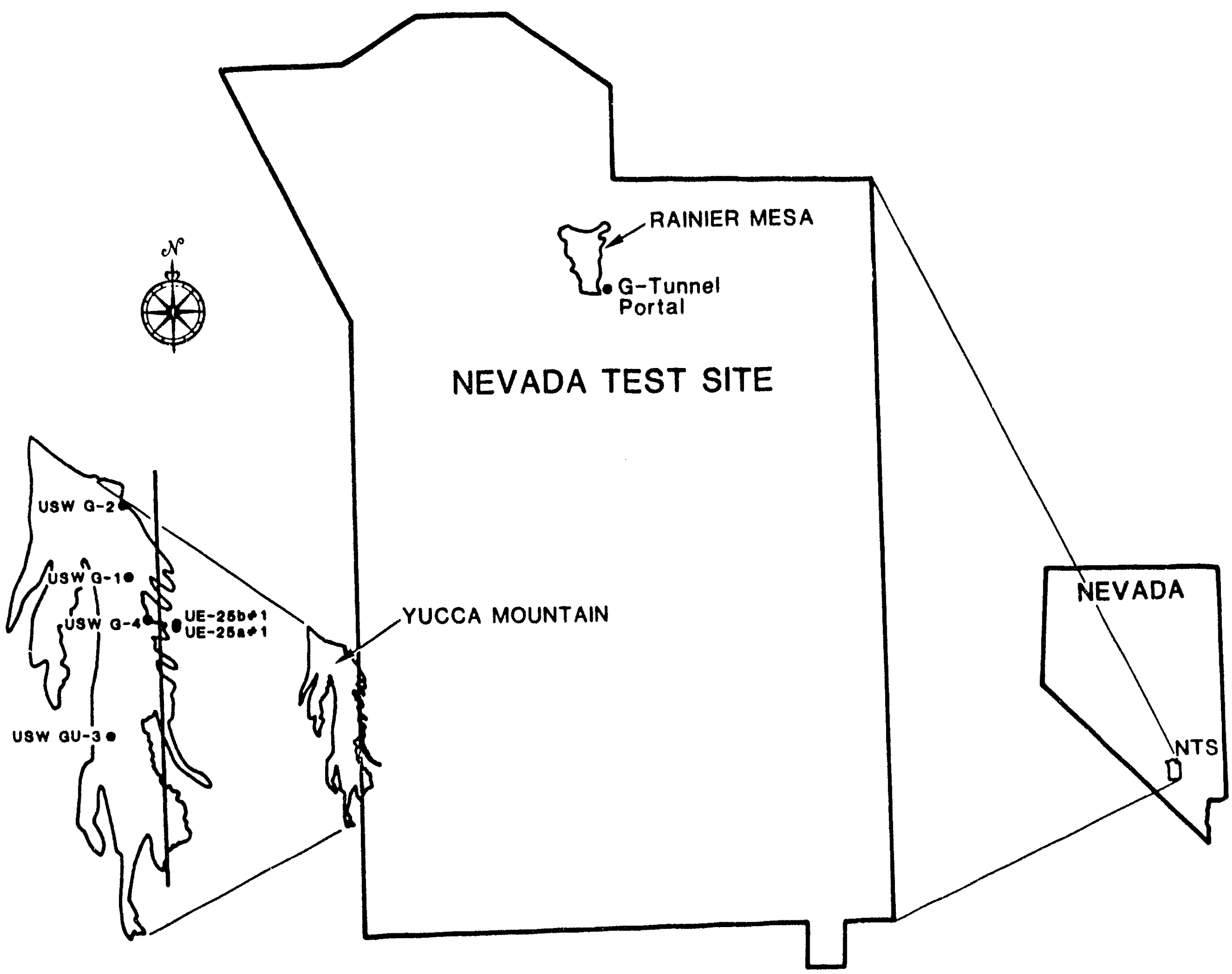

Figure 1: A map showing the Nevada test site and the relationship of Yucca Mountain with respect to the Nevada test site.

Table 1

Tuff Samples from Yucca Mountain: Modulus and Attenuation Measurements

Ultrasonic Experiments

Formation	Borehole depth, ft	Thermal/Mechanical Unit
Tiva Canyon	GU3-211.3	TCw
Tiva Canyon	GU3-165.35	TCw
Paintbrush tuff	G4-135.0	PTn
Paintbrush tuff	G2-709.7	PTn
Topopah Spring	G1-409.9	TSw1
Topopah Spring	G1-396.0	TSw1
Topopah Spring	G1-1157.5	TSw2
Topopah Spring	G1-906.0	TSw2
Topopah Spring	G1-721.4	TSw2
Calico Hills	G4-1617.75	CHn1z
Calico Hills	G1-1406.3	CHn1z
Topopah Spring	Busted Butte	TSw2

Resonant Bar Experiments

Tiva Canyon	GU3-165.35	TCw
Paintbrush Tuff	G4-135.0	PTn
Topopah Spring	Busted Butte	TSw2

Cyclic Loading Experiments

Tiva Canyon	Gu3-211.3	TCw
Topopah Spring	G1-409.9	TSw1
Calico Hills	G4-1617.75	CHn1z
Topopah Spring	Busted Butte	TSw2

Table 2.
Technique and Sample Dimensions

Technique	Frequency	Nominal Sample dimensions (mm) length	diameter
Cyclic loading	0.01 - 100 Hz	210	55
Waveform inversion	1 - 200 kHz	40	15
Resonant bar	1 - 200 kHz	201	13
Ultrasonic velocity	700 kHz	25	25

The quality and quantity of the rock determined the extent of the measurements on each lithology. Ultrasonic measurements were performed on all the specimens. The other techniques require larger specimens. It was not always possible to prepare cores of the appropriate dimensions; one sample of Topopah Spring Member (TSw2) tuff (BB-10AE-67-SNL-A) had sufficient material for all four techniques on both dry-and water-saturated specimens.

Specimens used for the cyclic loading, waveform inversion, and ultrasonic velocity measurements were right circular cylinders. The ends of all specimens were ground parallel to better than 5 x 10^{-4} mm/mm. The specimens for the resonant bar measurements were either slender rods 200 mm in length and 10 mm in diameter (GU3-165.35-SNL-B-2 and G4-135.0-SNL-B-1) or a bar 201 mm in length and 13 mm on a side (BB-10-AE-67-SNL-A). The specimen with a square cross section was first cut with a diamond saw to its approximate size and then ground to the final dimensions.

Prior to the deformation measurements, the dry bulk density and average grain density of each sample were measured. The grain densities were determined using a Micrometrics gas pycnometer. The porosities were computed from these data.

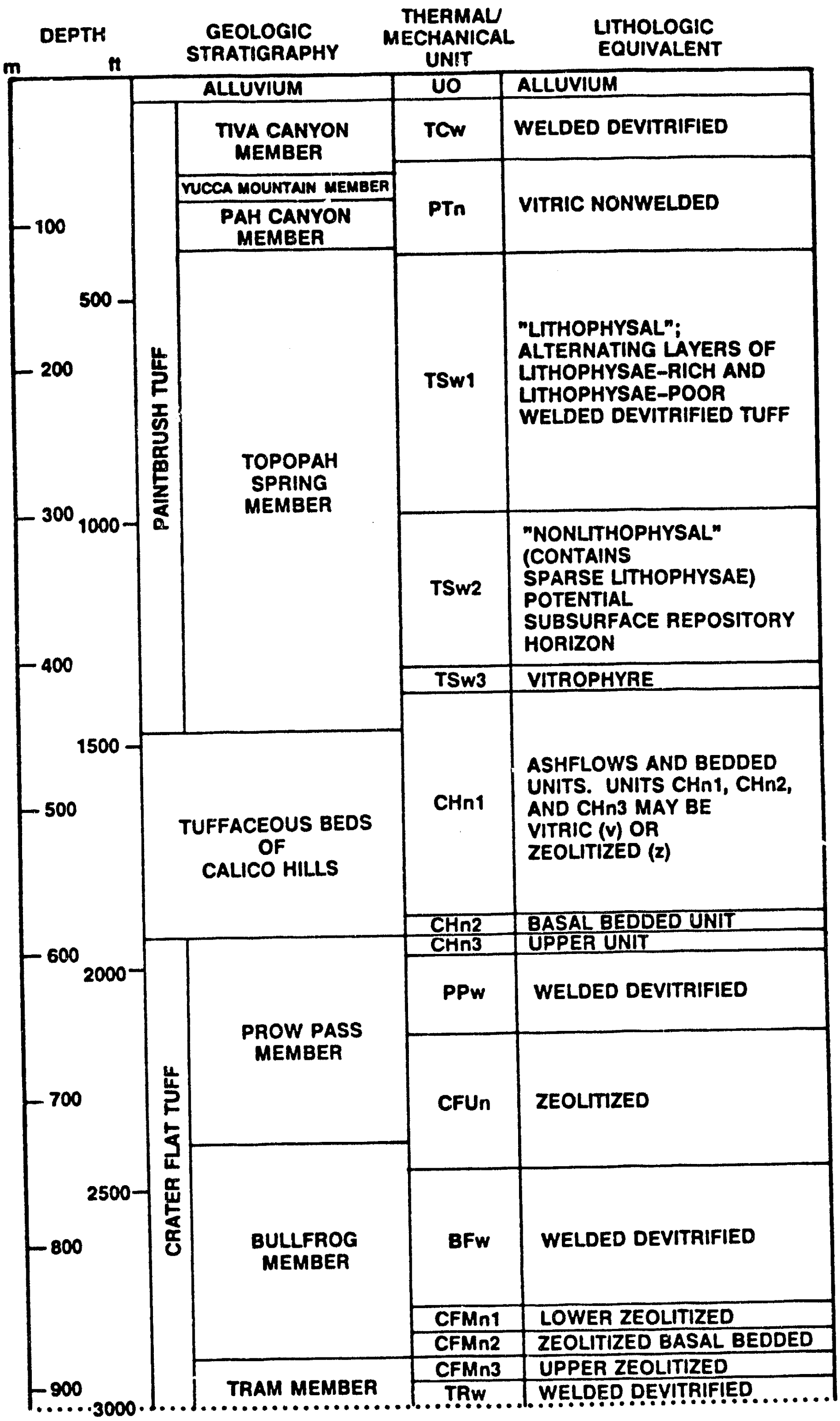

Figure 2: Comparison of geologic and thermal/mechanical stratigraphies of Yucca Mountain.

2.1 Cyclic Loading Experiments

A cyclic loading technique was used to investigate attenuation in the tuffs at low frequency and moderate to high strain amplitudes. In this technique, the sample is subjected to a continuous sinusoidal axial force while force and displacement are measured simultaneously.

Axial displacement of the specimen was measured with three LVDT displacement transducers mounted on two rings positioned near each end of the sample. The LVDT barrels were mounted in one ring, and the LVDT cores were attached to extension rods connected to the second ring. The axial displacement was the average of the three LVDTs. This sample assembly was positioned in series with a load cell in a hydraulic, servo-controlled loading frame. The sample was exposed to the atmosphere at room temperature and initially loaded to approximately 1 MPa. The specimen was loaded with a compressional sinusoidal axial force at frequencies between 10^{-2} and 10^{2} Hz. A function generator provided a reference signal for the system. Axial force from the load cell and sample displacement from the three LVDT transducers were measured and recorded with the PC-based data acquisition system.

Measurements were made at strain amplitudes between 10^{-6} and 10^{-4}. At each strain amplitude, the data were collected for 1 to 200 cycles. The strain was computed by dividing the displacement by the distance between the centers of the two mounting rings. Axial stress was calculated by dividing the measured load by the sample cross-sectional area.

Young's modulus and Q_E^{-1} were determined from the fast Fourier transforms of the stress and strain sinusoids. The modulus was calculated from the ratio of the peak amplitudes for the stress and strain spectrums at the driving frequency. Q_E^{-1} was computed in the frequency domain from the complex Young's modulus as given in Equation 3. Mechanical and electronic system losses were determined by conducting identical tests on a low loss standard (aluminum) with the same cross-sectional area and length as the rock specimens.

2.2 Waveform Inversion

Elastic wave velocities and attenuations were determined jointly for frequencies ranging from 10^3 to 2×10^5 Hz by using a waveform inversion technique based on the theory of low-frequency wave propagation along an elastic cylinder. This technique (Tang, 1992) compares the waveshapes obtained from measurements on two samples of the same material but having different lengths (which can be the same physical specimen, shortened for the second measurements). Using the low-frequency theory, we then estimated the elastic speeds and attenuation which most nearly account for the difference between the two waveforms. The waveform inversion technique was used only on dry and saturated specimens of the Topopah Spring Member (TSw2) tuff.

2.3 Resonant Bar Experiments

Benchtop resonant bar experiments were performed on three specimens of tuff, approximately 200 mm in length and 10 mm in diameter (Table 1), fully exposed to the atmosphere, and not previously dried. One specimen of TSw2 (BB-10AE-67-SNL-A) was also tested fully saturated. The saturated sample was wrapped with teflon tape to minimize evaporation losses.

The extensional resonance modes of the sample were excited with compressional piezoelectric ceramic crystals (10^6 Hz) epoxied to both sample ends (Figure 3). One crystal was arbitrarily identified as the excitation source and the other as the receiver. The sample was suspended in air with a fine thread attached to the sample at its midpoint. A phase lock amplifier was used to resonate the rod. Both source and sensing piezoelectric crystals were wired to the amplifier, one to the reference output and the second to the differential amplifier input. The differential amplifier input from the sensing crystal was able to "lock in" to the phase-shifted sine wave frequency being used to resonate the rod. A PC-controlled D/A converter was used as an external control for the phase lock amplifier reference sine wave output to sweep the frequency band of interest the amplified signal from the sensing crystal was measured as a function of frequency. Extensional wave attenuation was calculated by dividing frequency range at the half-power level (3 dB lower than resonance amplitude), Δf, by the center frequency, f_c.

$$Q_E^{-1} = \Delta f / f_c \tag{4}$$

Extensional (bar) velocity, V_E, was calculated by dividing the wavelength of the fundamental mode, which is twice the sample length, by the center frequency.

The extensional wave velocity is typically lower than the compressional wave velocity. The boundary conditions for a propagating wave in a long bar with free surfaces produce a

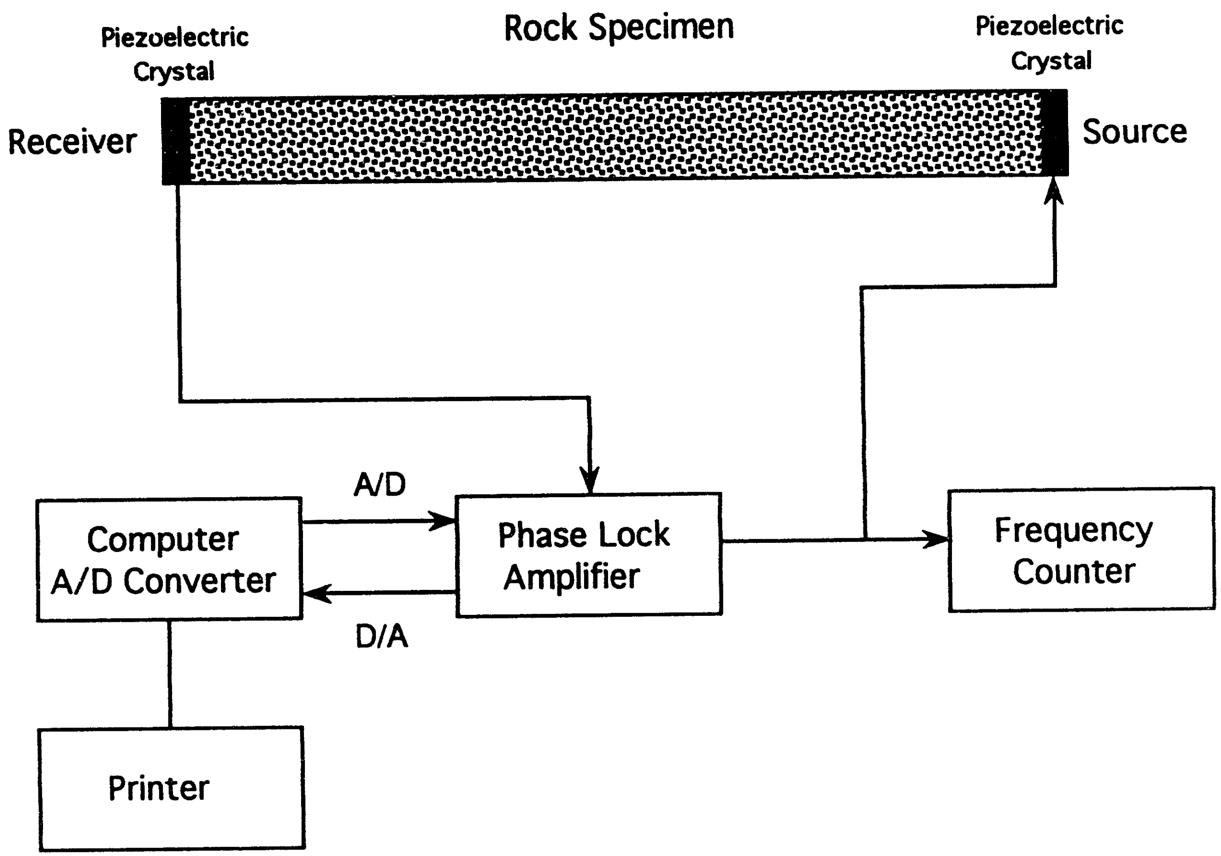

Figure 3: Schematic diagram of the benchtop resonant bar apparatus.

wave travelling at a lower velocity. The relationship between the compressional (longitudinal), V_p; shear, V_s; and extensional (bar) wave velocity, V_E, is

$$V_E = [V_s^2 (3 V_p^2 - 4V_s^2) / (V_p^2 - V_s^2)]^{0.5} \quad (5)$$

Young's modulus, E, was calculated from

$$E = \rho V_E^2 \quad (6)$$

where ρ is the density of the specimen.

The mass of the piezoelectric crystals and sample jacket were accounted for in a correction factor described by Lucet et al. (1991). Tittmann et al. (1980) and Lucet et al. (1991) discussed this technique in detail.

2.4 Ultrasonic Experiments

Ultrasonic velocity and attenuation measurements were performed on the thirteen samples of tuff. Broadband compressional (P) and shear (S) wave pulses, with maximum spectral amplitudes between 600 and 1200 kHz, were propagated through specimens nominally 25 mm in length by 25 mm in diameter. Measurements were carried out as a function of confining pressure for both room dry and saturated conditions at ambient laboratory temperatures (about 22° C). Velocities were calculated from the transit time of first arrivals. Attenuations were calculated with a spectral ratio technique (Toksöz et al., 1979) using 6061 aluminum as a high Q standard.

The apparatus used in the experiments included a source and receiver pair of like transducers (P, S1, or S2), a pulse generator, an amplifier, a filter, and a digital oscilloscope (Figure 4). The source crystal was excited by a fast risetime electrical pulse generated with a pulser-receiver. The crystal produced a broadband ultrasonic pulse that propagated through the adjacent titanium plate, through the rock sample along the core axis, through the titanium plate at the opposite end of the core, and into the receiver crystal. The electrical signal produced by the receiver transducer was amplified and filtered by the receiving section of the pulser-receiver, then digitized by an oscilloscope. The signals were typically amplified by 20 to 40 dB and high-pass filtered above 0.3 MHz. The oscilloscope displayed the signal for a travel time pick and the digitized signal was transferred to a computer for subsequent spectral attenuation analysis.

In a typical ultrasonic experiment, the sample is positioned between the source and receiver transducers, jacketed with polyolefin shrink tubing, and placed in a pressure vessel. A thin film of viscous resin couples the transducers to the sample for maximum

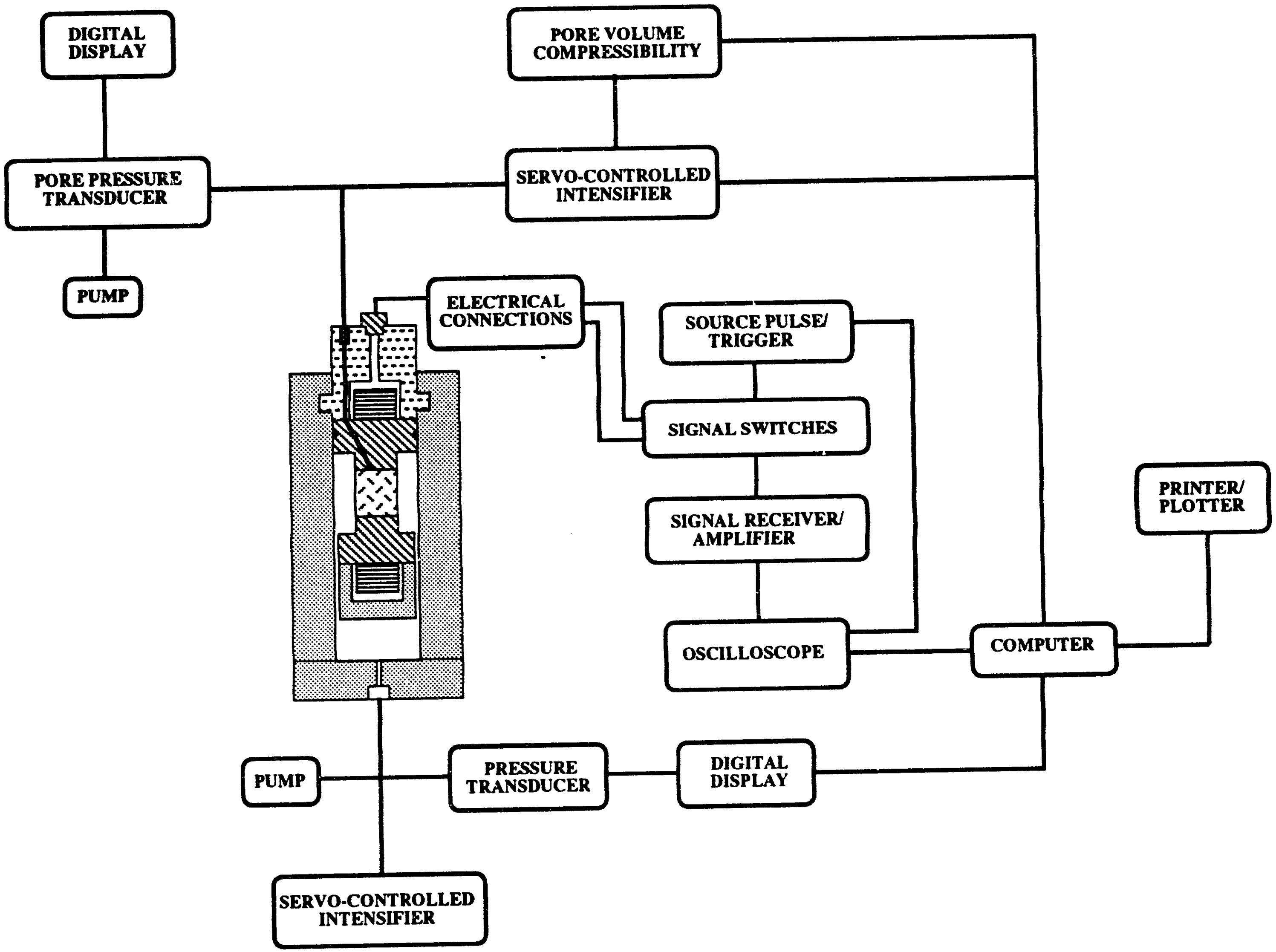

Figure 4: Schematic diagram of the experimental apparatus for ultrasonic velocity and attenuation measurements under pressure.

transmission of signals. The room dry measurements were always conducted first. The confining pressure was applied to the sample assembly and allowed to equilibrate for a period of approximately 10 minutes. Sequential P, S1, and S2 wave signals were propagated through the sample from source to receiver. Signals were displayed on the oscilloscope, travel times were picked, and the digitized signals were saved. Travel times were picked, with 10-nanosecond resolution, where a threshold voltage equal to 1.25% of the overall peak-to-peak amplitude of the received signal was exceeded. The entire sequence was repeated at successively higher confining pressures: 1.0, 2.5, 5.0, 7.5, 10.0, and 15.0 MPa.

After the dry measurements, the sample assembly was removed from the pressure vessel and the specimen was saturated with water. The saturated specimen was carefully jacketed and located between the transducers so as not to entrap any air, and the sample assembly was placed into the pressure vessel. Pore fluid pressure was externally controlled through a small port in one of the transducers. The first set of confining and pore fluid pressures, 3.5 MPa and 2.5 MPa, respectively, were applied to the specimen and allowed to equilibrate for a period of approximately 10 minutes. Ultrasonic measurements were then made in the same manner as for the dry samples. The sequence of confining pressures was 3.5, 5.0, 7.5, 10.0, 12.5, and 17.5 MPa. A constant pore pressure of 2.5 MPa was maintained. The effective confining pressure (confining pressure minus pore fluid pressure) was the same for both dry and saturated measurements.

Velocity and attenuation values for both P and S waves were calculated for the rock specimens at each confining pressure. Velocity was calculated by dividing specimen length by travel time through the rock. Specimen lengths were not corrected for strain under pressure because the resultant error in sample length was always less than 0.1%. Travel time through the sample was calculated by subtracting travel time through the titanium end pieces, from the total travel time.

Seismic attenuation was calculated using a spectral ratio technique. Two signals were recorded with the equipment settings exactly the same, one through the rock and the second through an aluminum standard of the same size. The digitized signals were displayed and windowed in the time domain over approximately two full cycles. The window edges were smoothed with a cosine taper. The two windowed signals were decomposed into amplitude versus frequency data utilizing standard Fourier analysis. The individual amplitude data and the natural logarithm of the ratio between them were displayed as functions of frequency. A least squares fit of the slope was made over a frequency band defined by 50% cutoffs of the peak signal amplitude in the frequency domain. The attenuation is given by

$$Q^{1} = \frac{\gamma V}{\pi} \tag{7}$$

where V is the measured velocity, and

$$\gamma = \ln\left(\frac{A_1}{A_2}\right) \tag{8}$$

where A_1 and A_2 are the spectral amplitudes for the aluminum standard and the rock respectively (Toksöz et al., 1979).

This method of measuring and calculating attenuation incorporates several assumptions. Attenuation is assumed to be constant over the frequency band of the signal, geometrical factors such as spreading and reflections are assumed constant for the two signals, and attenuation of the aluminum is assumed to be very small relative to the rock. The important variables in applying the technique included variations in window lengths, both in the time domain over which the ultrasonic signal was selected and in the frequency domain over which the spectral ratio slope was taken. The spectral ratio slope was normally well defined, although to a large extent this was achieved by interactively adjusting window lengths. A conservative estimate of error inherent in applying the technique is ± 25%.

3.0 EXPERIMENTAL RESULTS

One sample of Topopah Spring Member (TSw2) tuff, from a Busted Butte outcrop (BB-10-AE-67-SNL-A), was studied thoroughly. This was due to better sample availability, improved experimental technique as the project progressed, and the importance of the TSw2 as the potential repository rock. In light of the completeness of the data set and because it is the only rock on which all four experimental methods were performed, the results on these specimens are discussed separately.

The effect of frequency on Young's modulus and attenuation for the other tuff specimens is not as comprehensive. The data obtained on these rocks will be presented in terms of the experimental technique used to acquire the data.

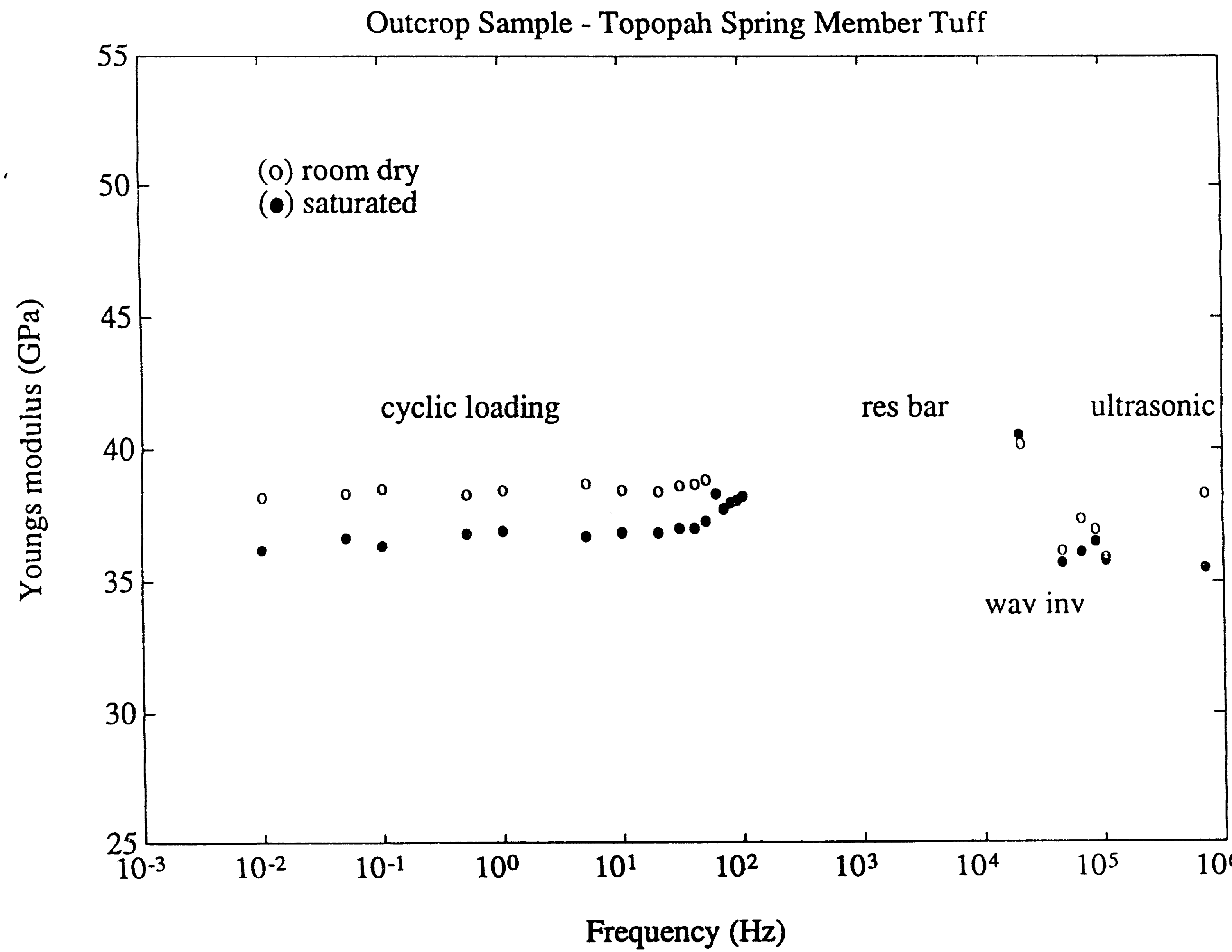

Figure 5: Young's modulus is shown as a function of frequency for a specimen of Topopah Spring Member tuff (TSw2) from the Busted Butte outcrop. All the measurements were performed at atmospheric pressure for dry and water saturated conditions.

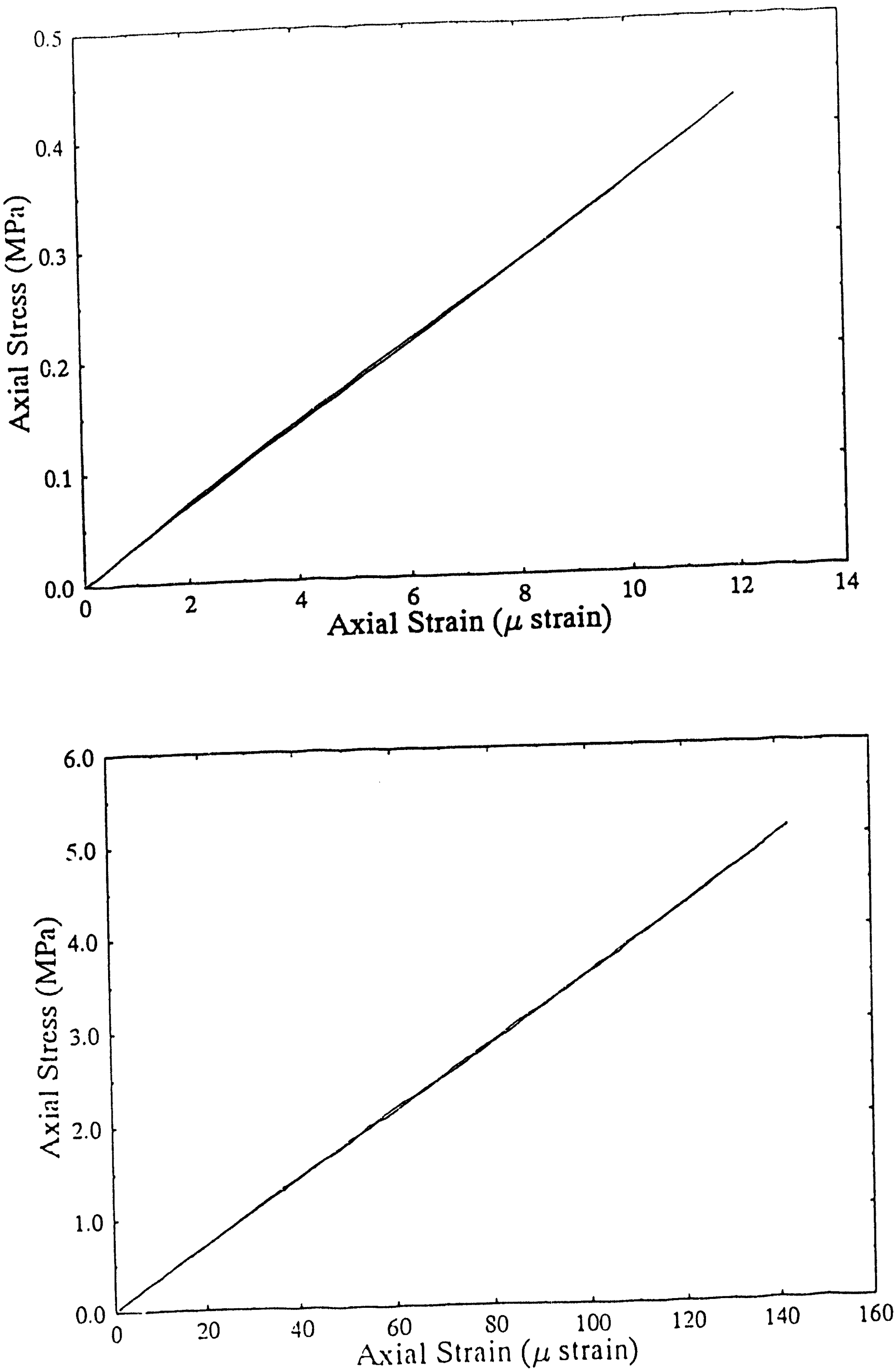

Figure 6: Axial stress is plotted as a function of axial strain for two cyclic loading experiments on a specimen of Topopah Spring Member tuff (TSw2) from the Busted Butte outcrop. The measurements were performed on a dry specimen at atmospheric pressure.

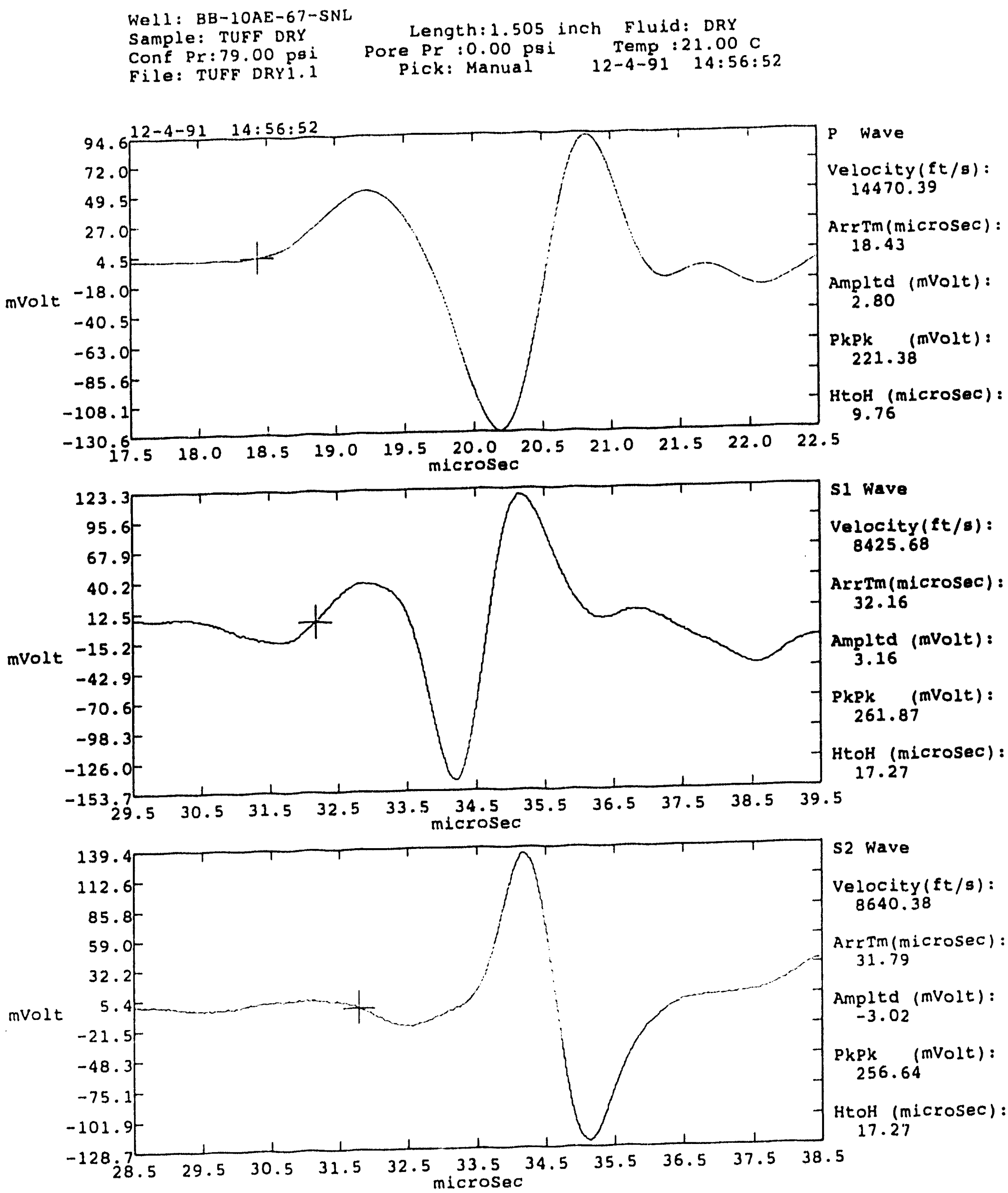

Figure 7: Compressional and shear wave time series plots for a specimen of Topopah Spring Member tuff (TSw2) from the Busted Butte outcrop. The measurements were obtained in a bench top apparatus under atmospheric conditions on a dry specimen.

3.1 Topopah Spring Member Tuff/Busted Butte Outcrop

The effects of frequency on Young's modulus for room-dry and water-saturated tuff are shown in Figure 5. Young's modulus for the dry tuff exhibits a small dependency on frequency between 10^{-2} and 10^{6} Hz. The cyclic loading measurements yielded a modulus of 38.2 GPa at 10^{-2} Hz. Young's modulus increased less than 2% as the frequency was increased to 50 Hz. Typical stress-strain curves for these measurements are shown in Figure 6. Axial stress is plotted as a function of axial strain for two strain amplitudes, 12 and 140 microstrain. An initial pre-load of 1 MPa was applied to the specimen prior to the cyclic loading measurements.

The modulus computed from the compressional and shear wave velocities is 38.3 GPa. This is in excellent agreement with the lower-frequency, cyclic loading measurements. The velocity data was collected in a benchtop apparatus with an applied stress of 1 MPa parallel to the wave propagation direction. Waveforms obtained for the tuff are shown in Figure 7. Three time series are shown; the top waveform is the compressional wave and the two lower waveforms are from the orthogonally polarized shear waves (S1 and S2).

The moduli computed using the resonant bar and waveform inversion techniques at about the same frequencies differ. For dry specimens, the Young's modulus computed from the first mode of the resonant bar measurements was 40.2 GPa at 20 kHz, whereas the waveform inversion method yielded a value of 36.2 GPa at 45 kHz.

The modulus for the water-saturated tuff was lower than the corresponding dry value at the same frequency by approximately 5%, except for the resonant bar where the modulus for the saturated specimen was 1% larger than for the dry condition. The values computed from the cyclic loading data exhibit noticeable dispersion at frequencies between 50 and 100 Hz. The effect of saturation on the moduli measured with the resonant bar and waveform inversion technique was small. For each technique, water saturation reduced the modulus.

Q_E^{-1} is shown as a function of frequency in Figure 8. For the dry condition, Q_E^{-1} is relatively low and independent of frequency below 50 Hz. The resonant bar attenuations, about 2.3 x 10^{-3}, are essentially the same as the cyclic loading measurements, 0.1 to 3.7 x 10^{-3}. The waveform inversion and the ultrasonic techniques yielded higher attenuations, averaging 19.5 x 10^{-3} and 23.5 x 10^{-3}, respectively.

The Q_E^{-1} in dry tuff was lower than that for the saturated conditions at corresponding frequencies. At frequencies below 10 Hz, the attenuation for the saturated state was

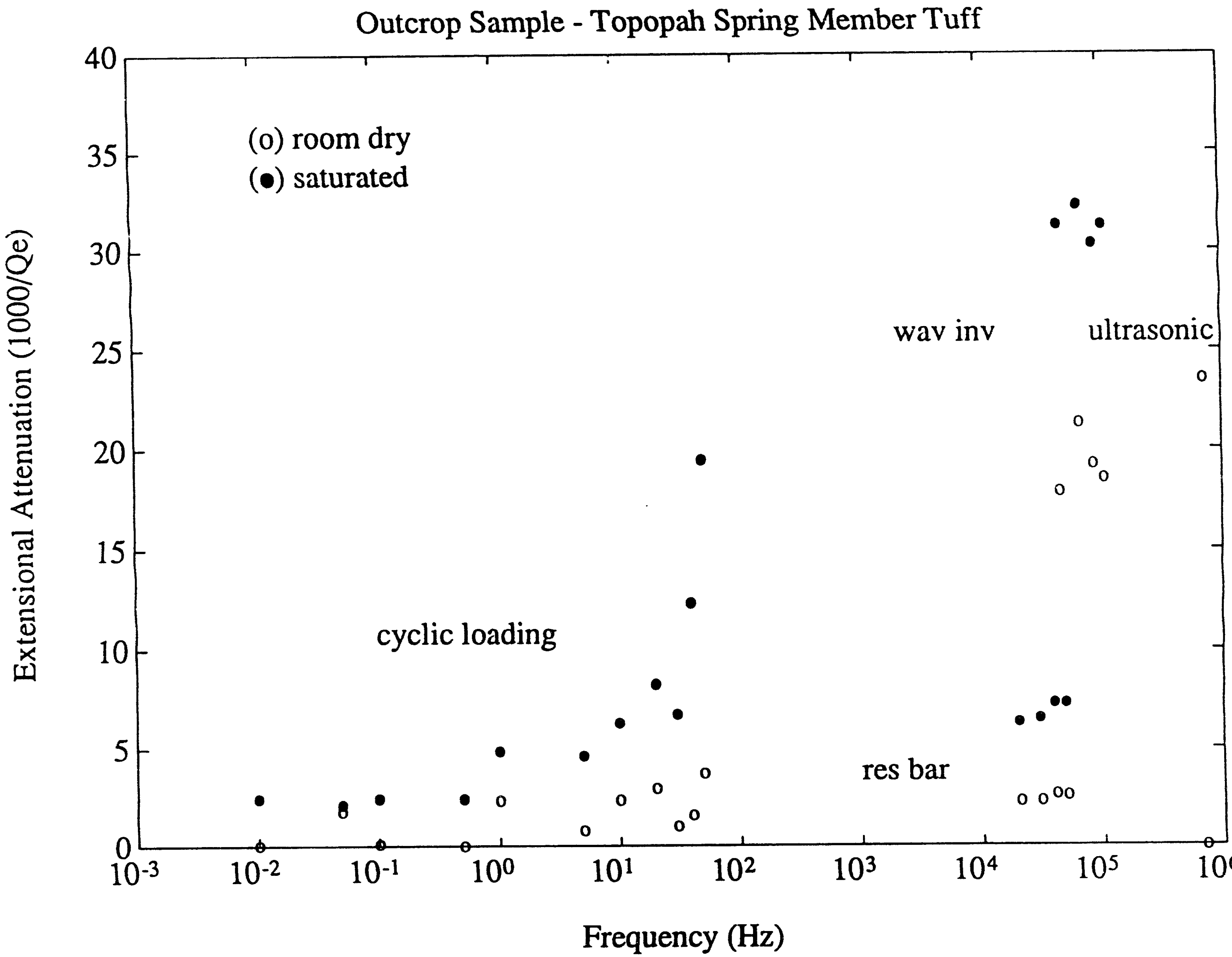

Figure 8: The attenuation for a specimen of Topopah Spring Member tuff (TSw2) from the Busted Butte outcrop is shown as a function of frequency. The measurements were carried out under atmospheric pressure. Data are shown for both dry and saturated states.

$3.2 \pm 1.7 \times 10^{-3}$. Between 10 and 10^2 Hz, the attenuation increased six-fold. A large difference between the attenuations measured with the waveform inversion and resonant bar methods was observed; the attenuations for the two methods at 5×10^4 Hz differed by a factor of five. No attenuation was calculated with the ultrasonic data from the saturated sample because of poor signal quality.

3.2 Partial Data Sets

3.2.1 Cyclic Loading

Cyclic loading experiments were performed on specimens of TCw, TSw1, TSw2, and CHn1 at atmospheric pressure, room temperature, at a frequency of 10^{-1} Hz. The results of these measurements are presented in Table 3. As an integral part of the cyclic loading experiments, the effect of strain amplitude was measured; typically strain amplitudes ranged from 5×10^{-7} to 8×10^{-5}. Figures 9a and 9b shows the effect of strain amplitude on Young's modulus and extensional attenuation for the TSw2 specimen (BB-10AE-67-SNL). This specimen was studied at both air dry and water-saturated conditions. As the strain amplitude increased, little variation in the Young's modulus was observed. Young's modulus for the dry condition exhibited a more or less constant value of 38.4 GPa at strains between 10^{-6} and 10^{-4}. Similarly, the moduli for the saturated conditions were independent of strain amplitude and exhibited values of 36.3 GPa. Attenuation for saturated specimens was generally larger than that for the dry state at corresponding strain amplitudes; however, there is an appreciable amount of scatter in the attenuation measurements. There is no consistent trend in attenuation with increasing strain amplitude for either the dry or saturated conditions.

Data from specimens of TCw, TSw1, and CHN1z are also given in Table 3. These experiments were carried out on air or room dry specimens only. The results from the Tiva Canyon (TCw) formation show that the Young's modulus decreases from 39.1 to 34.7 GPa as strain amplitude increased from 5×10^{-7} to 7.6×10^{6}. Over the same range of strain amplitudes, there is more than a five-fold increase in attenuation.

For the lithophysae-rich, TSw1, the effect of strain amplitude on modulus was small. Similarly, the attenuation showed only a small increase with increasing strain amplitude.

Table 3

Cyclic Loading measurements: Young's modulus and attenuation at 0.1 Hz

Unit	Sample	Strain Amplitude (microstrain)	Young's Modulus (GPa)	Extensional Attenuation (1000/Qe)
TCw	GU3-211.3-SNL-B	0.5	39.1	2.8
	Room dry	1.3	36.1	9.4
		3.99	35.3	10.2
		7.55	34.7	16.1
TSw1	G1-409.9-SNL-B	5.92	10.7	41.4
	Room dry	12.9	10.5	46.5
		22.9	11.0	57.6
		39.2	11.9	61.2
TSw2	BB-10-AE-67-SNL	2.7	38.3	2.5
	Room dry	7.3	38.3	1.7
		15.3	38.5	1.4
		53.1	38.4	2.6
		80.7	38.2	2.6
TSw2	BB-10-AE-67-SNL	6.1	36.0	4.1
	Water-saturated	10.1	36.3	1.9
		17.4	36.2	3.2
		31.0	36.1	3.6
		70.3	36.1	3.1
CHn1z	G4-1617.5-SNL-B	4.1	15.8	9.8
	Room dry	8.6	15.8	11.1
		15.6	15.8	12.8

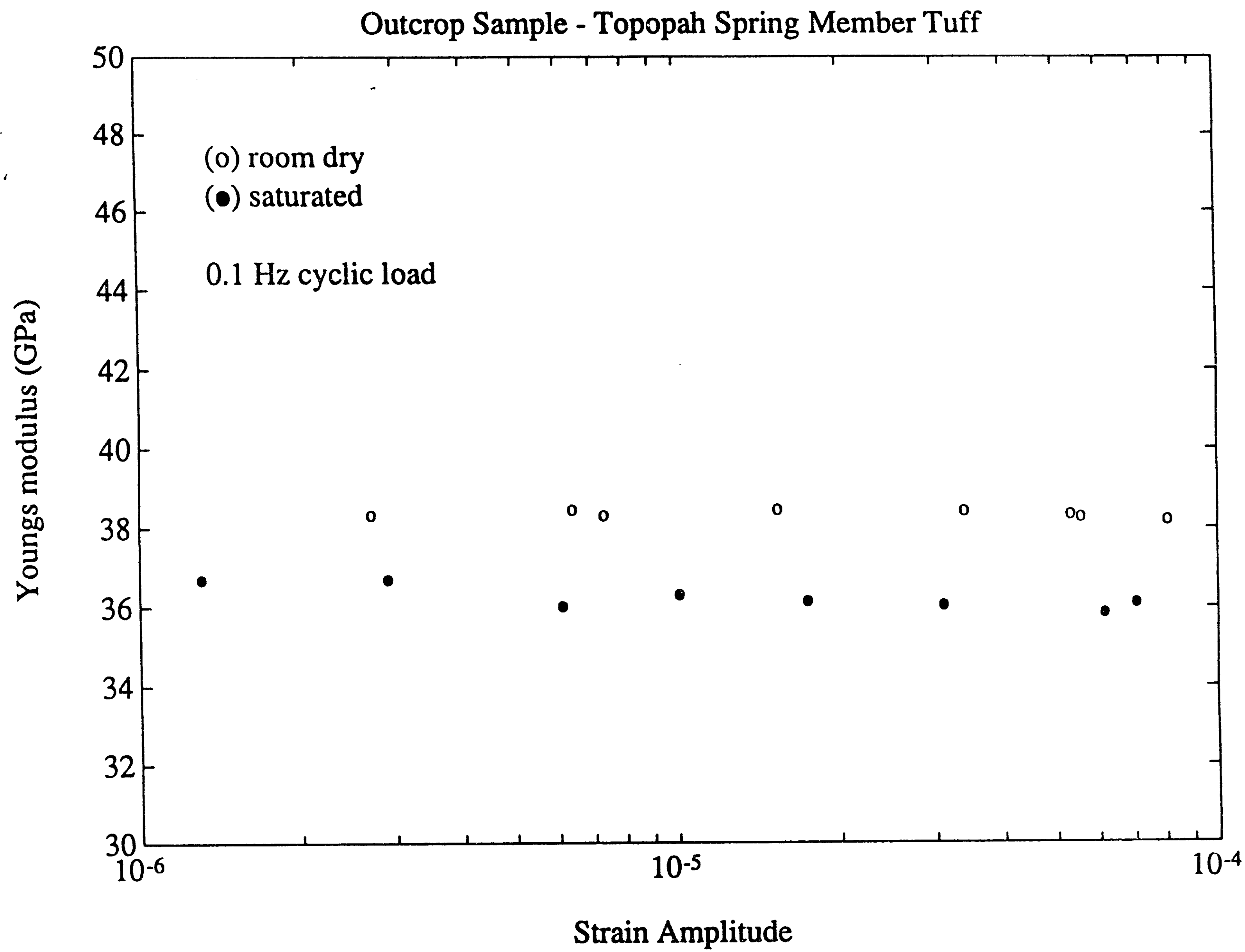

Figure 9a: Young's modulus is shown as functions of strain amplitude for a specimen of Topopah Spring Member tuff (TSw2). The data were collected on dry and saturated specimens at a frequency of 0.1 Hz at atmospheric pressure.

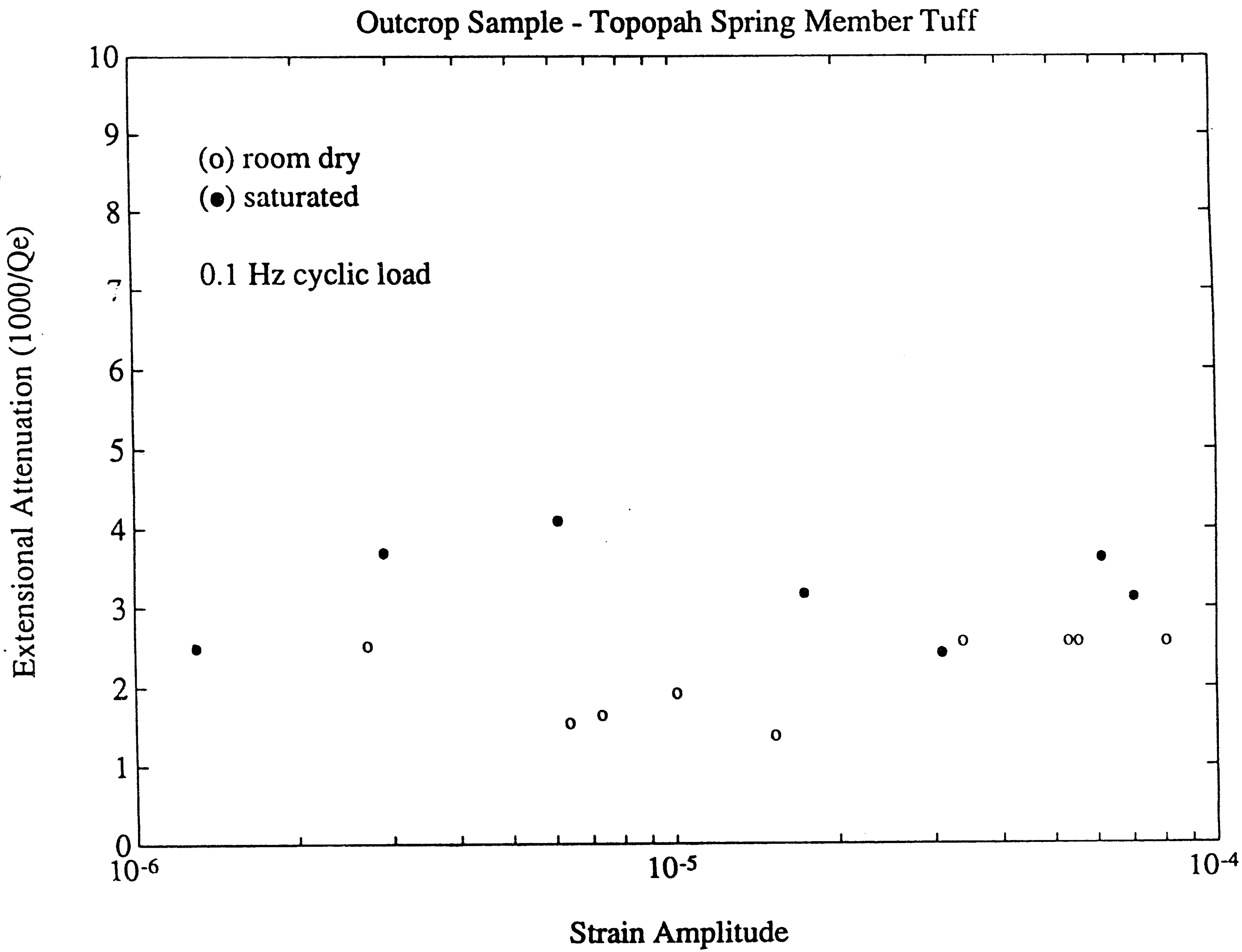

Figure 9b: Estensional attenuation is shown as functions of strain amplitude for a specimen of Topopah Spring Member tuff (TSw2). The data were collected on dry and saturated specimens at a frequency of 0.1 Hz at atmospheric pressure.

The tuff from the Calico Hills formation (CHn1z) showed no strain amplitude effect on Young's modulus. The extensional attenuation, Q_E^{-1}, increased from 9.8 x 10^{-3} to 12.8 x 10^{-3} as the strain amplitude was increased from 4 x 10^{-6} to 1.6 x 10^{-5}.

3.2.2 Resonant Bar

Resonant bar measurements were carried out on three specimens: one from the Topopah Spring Member (TSw2) tuff (the specimen discussed above), and one each from the Tiva Canyon (TCw) and the nonwelded Paintbrush (PTn) tuff units. These data are summarized in Table 4.

The resonant bar data collected for the Tiva Canyon (TCw) specimen (GU3-165.35-SNL-B-2) is shown in Figure 10. The amplitude of the measured signal is plotted as a function of frequency. The resonant peak was measured at 13.56 kHz. The attenuation for the specimen, computed using Equation 3, yielded a value of 1.1 x 10^{-3}. Young's modulus was computed as 35.7 GPa from the extensional wave velocity measured during the experiment.

Attenuation from resonant bar data for the specimen of PTn (G4-135.0-SNL-B), measured at a frequency of 5.28 kHz, was 5.4 x 10^{-3}; the corresponding Young's modulus was 6.8 GPa.

3.3 Ultrasonic Measurements

Much of the data for this study was collected using the ultrasonic technique. Compressional (longitudinal) and shear wave velocities were measured on each specimen as a function of confining pressure. The dry specimens were measured at pressures ranging from 1.0 to 15 MPa. In the saturated condition, velocities were determined at the same effective confining pressures, with a constant pore pressure of 2.5 MPa. Data on these specimens are given in Tables 5a through 5l. In each table, the compressional and shear wave velocities are listed as a function of confining pressure. In addition, the seismic wave attenuations are presented as a function of effective confining pressure. The attenuations for the compressional and shear waves are not directly comparable to the extensional attenuations, because the extensional wave velocity is lower than compressional wave velocity. Furthermore, Q_S^{-1}, the shear wave attenuation, has not been measured on any of the other specimens.

In general, the compressional and shear wave velocities exhibited a very small increase

Table 4

Resonant bar and waveform inversion measurements: Young's modulus and attenuation

Unit	Sample	Frequency (HZ)	Young's Modulus (GPa)	Extensional Attenuation (1000/Qe)
Resonant bar				
TCw	GU3-165.35-SNL-B-2 Room dry	13563	35.7	1.10
PTn	G4-135.0-SNL-B Room dry	5279	6.8	5.40
TSw2	BB-10AE-67-SNL Room dry	20,280	40.2	2.3
		30,155	39.0	2.3
		40,050	38.7	2.7
		49,667	37.7	2.7
TSw2	BB-10-AE-67-SNL Water-saturated	19,700	40.6	6.4
		29,400	39.9	6.6
		39,000	40.0	7.3
		48,400	40.4	7.3
Waveform Inversion				
TSw2	BB-10AE-67-SNL Room dry	45,000	36.2	17.9
		65,000	37.4	21.3
		85,000	37.0	19.2
		105,000	35.8	18.5
TSw2	BB-10AE-67-SNL Water-saturated	45,000	35.7	31.3
		65,000	36.1	32.3
		85,000	36.5	30.3
		105,000	35.9	31.3

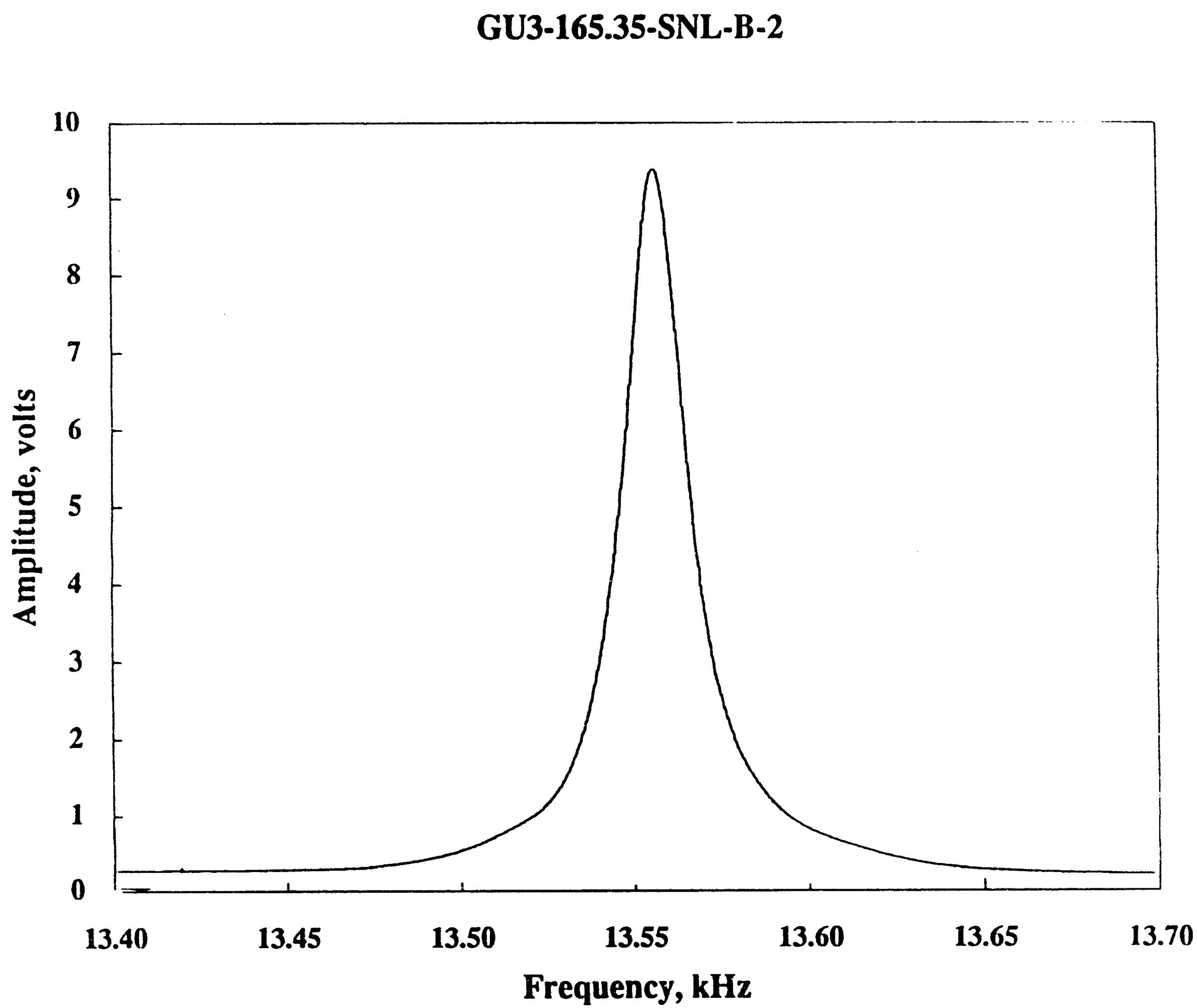

Figure 10: The output voltage from a resonant bar experiment on a specimen of Tiva Canyon tuff is presented. The output amplitude is plotted as a function of frequency; the resonant peak occurs at a frequency near 13.56 kHz.

with increasing confining pressure for both dry and saturated conditions. In most instances, the compressional wave velocity measured on the saturated specimens was greater than that observed on the dry specimen. Shear wave velocity for the saturated specimen was less than that observed for the dry state. The attenuations, Q_P^{-1} and Q_S^{-1}, also showed a very small dependence on confining pressure. In most cases the attenuation decreased with increasing confining pressure up to 15 MPa. The data collected on the Tiva Canyon Member (TCw) specimen (GU3-211.3-SNL-A2) are shown graphically in Figures 11a and 11b. The compressional and shear wave velocities as well as the corresponding attenuations are plotted as a function of effective confining pressure. This specimen has a low porosity of 1.9%. In contrast, a nonwelded specimen of PTn (G2-709.7-SNL-B), with a porosity of 48%, showed a pronounced pressure dependence for the compressional wave velocity (most apparent for the dry condition), a small pressure dependence for the shear wave velocity, and attenuations that were independent of confining pressure. These data are shown in Figures 12a and 12b.

Table 5a

Ultrasonic compressional and shear wave velocities and associated seismic attenuations for dry and water saturated conditions as a function of confining pressure

SAMPLE ID:	G1-396.0-SNL-A-1
ORIENTATION:	VERTICAL
PORE FLUID:	DRY/WATER
TEMPERATURE, ° C:	22
SAMPLE LENGTH, mm:	25.43
SAMPLE DIAMETER, mm:	24.84
VACUUM DRY WEIGHT, g:	26.086
ROOM DRY WEIGHT, g:	26.101
SAT WEIGHT, g:	28.064
DRY BULK DENSITY, g/cm^3:	2.117
POROSITY, %:	16.1

PRESSURE (MPa)			VELOCITY (km/s^{-1})			VP/VS	1000/Q	
CONF	PORE	DIFF	P-WAVE	S1-WAVE	S2-WAVE	RATIO	P-WAVE	S2-WAVE
ROOM DRY								
1.0	0.0	1.0	4.028	2.473	2.630	1.58	63	102
2.5	0.0	2.5	4.054	2.507	2.646	1.57	61	99
5.0	0.0	5.0	4.106	2.553	2.697	1.56	59	93
7.5	0.0	7.5	4.146	2.568	2.720	1.57	56	85
10.0	0.0	10.0	4.160	2.594	2.743	1.56	54	84
15.0	0.0	15.0	4.187	2.610	2.761	1.56	52	83
SATURATED								
3.5	2.5	1.0	4.443	2.346	2.301	1.91	102	156
5.0	2.5	2.5	4.459	2.381	2.331	1.89	102	153
7.5	2.5	5.0	4.483	2.421	2.379	1.87	102	143
10.0	2.5	7.5	4.498	2.454	2.406	1.85	102	135
12.5	2.5	10.0	4.506	2.473	2.438	1.84	100	111
17.5	2.5	15.0	4.522	2.498	2.452	1.83	80	94

COMMENT: Shear wave polarization randomly oriented.

Table 5b

Ultrasonic compressional and shear wave velocities and associated seismic attenuations for dry and water saturated conditions as a function of confining pressure

SAMPLE ID:	G1-409.9-SNL-A-1
ORIENTATION:	VERTICAL
PORE FLUID:	DRY/WATER
TEMPERATURE, ° C:	22
SAMPLE LENGTH, mm:	25.40
SAMPLE DIAMETER, mm:	24.56
VACUUM DRY WEIGHT, g:	26.860
ROOM DRY WEIGHT, g:	26.999
SAT WEIGHT, g:	28.508
DRY BULK DENSITY, g/cm^3:	2.232
POROSITY, %:	13.7

PRESSURE (MPa)			VELOCITY (km/s^{-1})			VP/VS	1000/Q	
CONF	PORE	DIFF	P-WAVE	S1-WAVE	S2-WAVE	RATIO	P-WAVE	S2-WAVE
ROOM DRY								
1.0	0.0	1.0	4.197	2.522	2.455	1.69	159	123
2.5	0.0	2.5	4.225	2.535	2.464	1.69	158	122
5.0	0.0	5.0	4.246	2.548	2.479	1.69	156	123
7.5	0.0	7.5	4.267	2.558	2.488	1.69	152	123
10.0	0.0	10.0	4.275	2.566	2.493	1.69	143	120
15.0	0.0	15.0	4.289	2.573	2.503	1.69	135	115
SATURATED								
3.5	2.5	1.0	4.447	2.535	2.498	1.77	154	120
5.0	2.5	2.5	4.462	2.540	2.498	1.77	154	120
7.5	2.5	5.0	4.462	2.550	2.503	1.77	152	119
10.0	2.5	7.5	4.478	2.555	2.505	1.77	147	116
12.5	2.5	10.0	4.486	2.560	2.510	1.77	146	116
17.5	2.5	15.0	4.494	2.568	2.513	1.77	146	114

COMMENT: Shear wave polarization randomly oriented.

Table 5c

Ultrasonic compressional and shear wave velocities and associated seismic attenuations for dry and water saturated conditions as a function of confining pressure

SAMPLE ID:	G1-409.9-SNL-A-2
ORIENTATION:	VERTICAL
PORE FLUID:	DRY/WATER
TEMPERATURE, ° C:	22
SAMPLE LENGTH, mm:	25.40
SAMPLE DIAMETER, mm:	24.51
VACUUM DRY WEIGHT, g:	26.386
ROOM DRY WEIGHT, g:	
SAT WEIGHT, g:	27.873
DRY BULK DENSITY, g/cm³:	2.202
POROSITY, %:	12.4

PRESSURE (MPa)			VELOCITY (km/s^{-1})			VP/VS	1000/Q	
CONF	PORE	DIFF	P-WAVE	S1-WAVE	S2-WAVE	RATIO	P-WAVE	S2-WAVE
ROOM DRY								
1.0	0.0	1.0	4.163	2.517	2.479	1.67	102	133
2.5	0.0	2.5	4.183	2.532	2.493	1.66	102	133
5.0	0.0	5.0	4.211	2.548	2.508	1.67	102	133
7.5	0.0	7.5	4.225	2.555	2.518	1.67	102	133
10.0	0.0	10.0	4.239	2.563	2.528	1.67	102	133
15.0	0.0	15.0	4.253	2.573	2.538	1.66	101	133
SATURATED								
3.5	2.5	1.0	4.439	2.525	2.486	1.77	120	111
5.0	2.5	2.5	4.447	2.527	2.491	1.77	120	111
7.5	2.5	5.0	4.447	2.543	2.503	1.76	118	114
10.0	2.5	7.5	4.445	2.553	2.508	1.76	119	114
12.5	2.5	10.0	4.462	2.558	2.518	1.75	119	97
17.5	2.5	15.0	4.462	2.566	2.523	1.77	119	97

COMMENT: Shear wave polarization randomly oriented.

Table 5d

Ultrasonic compressional and shear wave velocities and associated seismic attenuations for dry and water saturated conditions as a function of confining pressure

SAMPLE ID:	G1-721.4-SNL-A-1
ORIENTATION:	VERTICAL
PORE FLUID:	DRY/WATER
TEMPERATURE, ° C:	22
SAMPLE LENGTH, mm:	25.43
SAMPLE DIAMETER, mm:	24.82
VACUUM DRY WEIGHT, g:	27.752
ROOM DRY WEIGHT, g:	27.767
SAT WEIGHT, g:	28.632
DRY BULK DENSITY, g/cm^3:	2.257
POROSITY, %:	7.2

PRESSURE (MPa)			VELOCITY (km/s^{-1})			VP/VS	1000/Q	
CONF	PORE	DIFF	P-WAVE	S1-WAVE	S2-WAVE	RATIO	P-WAVE	S2-WAVE
ROOM DRY								
1.0	0.0	1.0	4.337	2.740	2.735	1.58	30	62
2.5	0.0	2.5	4.345	2.749	2.746	1.58	30	62
5.0	0.0	5.0	4.360	2.758	2.752	1.58	29	61
7.5	0.0	7.5	4.360	2.764	2.758	1.58	29	56
10.0	0.0	10.0	4.367	2.767	2.758	1.58	29	52
15.0	0.0	15.0	4.367	2.773	2.764	1.58	25	52
SATURATED								
3.5	2.5	1.0	4.397	2.685	2.735	1.62	53	89
5.0	2.5	2.5	4.405	2.708	2.697	1.63	49	89
7.5	2.5	5.0	4.413	2.693	2.697	1.64	48	83
10.0	2.5	7.5	4.428	2.699	2.703	1.64	44	71
12.5	2.5	10.0	4.428	2.702	2.705	1.64	44	65
17.5	2.5	15.0	4.436	2.708	2.708	1.64	45	61

COMMENT: Shear wave polarization randomly oriented.

Table 5e

Ultrasonic compressional and shear wave velocities and associated seismic attenuations for dry and water saturated conditions as a function of confining pressure

SAMPLE ID:	G1-906.0-SNL-B-1
ORIENTATION:	HORIZONTAL
PORE FLUID:	DRY/WATER
TEMPERATURE, °C:	22
SAMPLE LENGTH, mm:	25.40
SAMPLE DIAMETER, mm:	24.87
VACUUM DRY WEIGHT, g:	28.201
ROOM DRY WEIGHT, g:	28.202
SAT WEIGHT, g:	29.341
DRY BULK DENSITY, g/cm^3:	2.286
POROSITY, %:	9.2

PRESSURE (MPa)			VELOCITY (km/s^{-1})			VP/VS	1000/Q	
CONF	PORE	DIFF	P-WAVE	S1-WAVE	S2-WAVE	RATIO	P-WAVE	S2-WAVE
ROOM DRY								
1.0	0.0	1.0	4.416	2.691	2.720	1.63	105	100
2.5	0.0	2.5	4.431	2.711	2.732	1.63	97	86
5.0	0.0	5.0	4.462	2.737	2.750	1.63	83	79
7.5	0.0	7.5	4.486	2.752	2.758	1.63	72	74
10.0	0.0	10.0	4.502	2.758	2.767	1.63	67	71
15.0	0.0	15.0	4.510	2.770	2.774	1.63	58	70
SATURATED								
3.5	2.5	1.0	4.608	2.758	2.700	1.69	74	100
5.0	2.5	2.5	4.608	2.764	2.714	1.68	70	98
7.5	2.5	5.0	4.625	2.761	2.711	1.69	68	96
10.0	2.5	7.5	4.642	2.740	2.717	1.70	63	94
12.5	2.5	10.0	4.659	2.746	2.726	1.70	61	83
17.5	2.5	15.0	4.667	2.761	2.738	1.70	60	77

COMMENT: Shear wave polarization randomly oriented.

Table 5f

Ultrasonic compressional and shear wave velocities and associated seismic attenuations for dry and water saturated conditions as a function of confining pressure

SAMPLE ID:	G1-1157.5-SNL-A-1
ORIENTATION:	VERTICAL
PORE FLUID:	DRY/WATER
TEMPERATURE, ° C:	22
SAMPLE LENGTH, mm:	25.65
SAMPLE DIAMETER, mm:	24.59
VACUUM DRY WEIGHT, g:	28.043
ROOM DRY WEIGHT, g:	28.136
SAT WEIGHT, g:	29.055
DRY BULK DENSITY, g/cm^3:	2.302
POROSITY, %:	8.3

PRESSURE (MPa)			VELOCITY (km/s^{-1})			VP/VS	1000/Q	
CONF	PORE	DIFF	P-WAVE	S1-WAVE	S2-WAVE	RATIO	P-WAVE	S2-WAVE
ROOM DRY								
1.0	0.0	1.0	3.970	2.658	2.587	1.51	104	45
2.5	0.0	2.5	4.013	2.658	2.600	1.53	118	45
5.0	0.0	5.0	4.026	2.658	2.621	1.53	119	43
7.5	0.0	7.5	4.020	2.661	2.626	1.52	118	43
10.0	0.0	10.0	4.032	2.672	2.648	1.52	111	42
15.0	0.0	15.0	4.090	2.686	2.665	1.53	110	41
SATURATED								
3.5	2.5	1.0	4.289	2.594	2.551	1.67	69	49
5.0	2.5	2.5	4.296	2.602	2.561	1.66	68	48
7.5	2.5	5.0	4.296	2.602	2.566	1.66	66	48
10.0	2.5	7.5	4.310	2.604	2.571	1.67	65	47
12.5	2.5	10.0	4.317	2.607	2.579	1.67	63	46
17.5	2.5	15.0	4.339	2.618	2.587	1.67	62	46

COMMENT: Shear wave polarization randomly oriented.

Table 5g

Ultrasonic compressional and shear wave velocities and associated seismic attenuations for dry and water saturated conditions as a function of confining pressure

SAMPLE ID:	G1-1406.3-SNL-A-1
ORIENTATION:	VERTICAL
PORE FLUID:	DRY/WATER
TEMPERATURE, ° C:	22
SAMPLE LENGTH, mm:	25.30
SAMPLE DIAMETER, mm:	22.22
VACUUM DRY WEIGHT, g:	14.544
ROOM DRY WEIGHT, g:	14.804
SAT WEIGHT, g:	18.01
DRY BULK DENSITY, g/cm^3:	1.482
POROSITY, %:	35.3

PRESSURE (MPa)			VELOCITY (km/s^{-1})			VP/VS	1000/Q	
CONF	PORE	DIFF	P-WAVE	S1-WAVE	S2-WAVE	RATIO	P-WAVE	S2-WAVE
ROOM DRY								
1.0	0.0	1.0						
2.5	0.0	2.5						
5.0	0.0	5.0						
7.5	0.0	7.5	2.563	1.511	1.507	1.70	310	156
10.0	0.0	10.0	2.573	1.531	1.529	1.68	310	147
15.0	0.0	15.0	2.605	1.558	1.561	1.67	310	139
SATURATED								
3.5	2.5	1.0	2.688	1.009	1.010	2.66	272	108
5.0	2.5	2.5	2.699	1.014	1.015	2.66	270	83
7.5	2.5	5.0	2.723	1.023	1.026	2.66	262	68
10.0	2.5	7.5	2.770	1.033	1.036	2.68	256	63
12.5	2.5	10.0	2.776	1.044	1.047	2.66	241	57
17.5	2.5	15.0	2.839	1.065	1.065	2.67	241	56

COMMENT: Poor signal at low confining pressures. Unable to define first break of signal for dry sample measurements.

Table 5h

Ultrasonic compressional and shear wave velocities and associated seismic attenuations for dry and water saturated conditions as a function of confining pressure

SAMPLE ID:	G2-709.7-SNL-B-1
ORIENTATION:	HORIZONTAL
PORE FLUID:	DRY/WATER
TEMPERATURE, ° C:	22
SAMPLE LENGTH, mm:	25.60
SAMPLE DIAMETER, mm:	23.16
VACUUM DRY WEIGHT, g:	13.646
ROOM DRY WEIGHT, g:	14.556
SAT WEIGHT, g:	18.834
DRY BULK DENSITY, g/cm^3:	1.265
POROSITY, %:	48.1

PRESSURE (MPa)			VELOCITY (km/s^{-1})			VP/VS	1000/Q	
CONF	PORE	DIFF	P-WAVE	S1-WAVE	S2-WAVE	RATIO	P-WAVE	S2-WAVE
ROOM DRY								
1.0	0.0	1.0	1.619	1.006	1.006	1.61	315	59
2.5	0.0	2.5	1.640	1.010	1.011	1.62	315	56
5.0	0.0	5.0	2.086	1.018	1.023	2.04	315	56
7.5	0.0	7.5	2.263	1.022	1.025	2.21	315	54
10.0	0.0	10.0	2.372	1.034	1.032	2.30	315	53
15.0	0.0	15.0	2.431	1.047	1.050	2.32	315	53
SATURATED								
3.5	2.5	1.0	2.351	1.021	1.029	2.29	313	59
5.0	2.5	2.5	2.404	1.024	1.034	2.34	310	59
7.5	2.5	5.0	2.483	1.032	1.043	2.39	286	60
10.0	2.5	7.5	2.542	1.042	1.053	2.43	251	60
12.5	2.5	10.0	2.578	1.053	1.075	2.42	238	26
17.5	2.5	15.0	2.675	1.091	1.103	2.44	228	52

COMMENT: Shear wave polarization randomly oriented.
Sample became disintegrated upon saturation.

Table 5i

Ultrasonic compressional and shear wave velocities and associated seismic attenuations for dry and water saturated conditions as a function of confining pressure

SAMPLE ID:	GU3-165.35-SNL-A-1
ORIENTATION:	VERTICAL
PORE FLUID:	DRY/WATER
TEMPERATURE, ° C:	22
SAMPLE LENGTH, mm:	25.43
SAMPLE DIAMETER, mm:	24.59
VACUUM DRY WEIGHT, g:	27.389
ROOM DRY WEIGHT, g:	27.396
SAT WEIGHT, g:	28.209
DRY BULK DENSITY, g/cm^3:	2.269
POROSITY, %:	6.8

PRESSURE (MPa)			VELOCITY (km/s^{-1})			VP/VS	1000/Q	
CONF	PORE	DIFF	P-WAVE	S1-WAVE	S2-WAVE	RATIO	P-WAVE	S2-WAVE
ROOM DRY								
1.0	0.0	1.0	4.630	2.822	2.832	1.64	97	97
2.5	0.0	2.5	4.646	2.834	2.848	1.64	97	94
5.0	0.0	5.0	4.655	2.841	2.857	1.63	97	89
7.5	0.0	7.5	4.663	2.844	2.861	1.63	96	85
10.0	0.0	10.0	4.663	2.847	2.864	1.63	96	81
15.0	0.0	15.0	4.672	2.854	2.874	1.63	96	78
SATURATED								
3.5	2.5	1.0	4.663	2.806	2.810	1.66	65	109
5.0	2.5	2.5	4.681	2.809	2.816	1.66	64	106
7.5	2.5	5.0	4.689	2.816	2.832	1.66	61	91
10.0	2.5	7.5	4.698	2.822	2.835	1.66	59	83
12.5	2.5	10.0	4.698	2.825	2.841	1.66	56	77
17.5	2.5	15.0	4.707	2.831	2.848	1.66	52	71

COMMENT: Shear wave polarization randomly oriented.

Table 5j

Ultrasonic compressional and shear wave velocities and associated seismic attenuations for dry and water saturated conditions as a function of confining pressure

SAMPLE ID:	GU3-211.3-SNL-A-2
ORIENTATION:	VERTICAL
PORE FLUID:	DRY/WATER
TEMPERATURE, ° C:	22
SAMPLE LENGTH, mm:	25.43
SAMPLE DIAMETER, mm:	24.82
VACUUM DRY WEIGHT, g:	28.6
ROOM DRY WEIGHT, g:	28.62
SAT WEIGHT, g:	28.837
DRY BULK DENSITY, g/cm^3:	2.326
POROSITY, %:	1.9

PRESSURE (MPa)			VELOCITY (km/s^{-1})			VP/VS	1000/Q	
CONF	PORE	DIFF	P-WAVE	S1-WAVE	S2-WAVE	RATIO	P-WAVE	S2-WAVE
ROOM DRY								
1.0	0.0	1.0	4.724	2.929	2.937	1.61	71	82
2.5	0.0	2.5	4.733	2.936	2.940	1.61	71	82
5.0	0.0	5.0	4.733	2.943	2.947	1.61	71	77
7.5	0.0	7.5	4.742	2.946	2.950	1.61	66	75
10.0	0.0	10.0	4.751	2.950	2.954	1.61	66	71
15.0	0.0	15.0	4.760	2.953	2.957	1.61	68	69
SATURATED								
3.5	2.5	1.0	4.689	2.899	2.893	1.62	87	65
5.0	2.5	2.5	4.715	2.906	2.896	1.63	87	65
7.5	2.5	5.0	4.724	2.916	2.906	1.62	85	64
10.0	2.5	7.5	4.724	2.922	2.910	1.62	83	62
12.5	2.5	10.0	4.733	2.929	2.916	1.62	83	60
17.5	2.5	15.0	4.724	2.936	2.920	1.62	81	56

COMMENT: Shear wave polarization randomly oriented.

Table 5k

Ultrasonic compressional and shear wave velocities and associated seismic attenuations for dry and water saturated conditions as a function of confining pressure

SAMPLE ID:	G4-135-0-SNL-A-1
ORIENTATION:	VERTICAL
PORE FLUID:	DRY/WATER
TEMPERATURE, ° C:	22
SAMPLE LENGTH, mm:	25.73
SAMPLE DIAMETER, mm:	22.48
VACUUM DRY WEIGHT, g:	14.193
ROOM DRY WEIGHT, g:	14.256
SAT WEIGHT, g:	17.817
DRY BULK DENSITY, g/cm^3:	1.390
POROSITY, %:	35.5

PRESSURE (MPa)			VELOCITY (km/s^{-1})			VP/VS	1000/Q	
CONF	PORE	DIFF	P-WAVE	S1-WAVE	S2-WAVE	RATIO	P-WAVE	S2-WAVE
ROOM DRY								
1.0	0.0	1.0					145	94
2.5	0.0	2.5	2.175	1.243	1.295	1.71	145	94
5.0	0.0	5.0	2.332	1.489	1.412	1.61	145	94
7.5	0.0	7.5	2.486	1.584	1.424	1.65	145	94
10.0	0.0	10.0	2.596	1.624	1.471	1.68	145	94
15.0	0.0	15.0	2.716	1.680	1.534	1.69	145	94
SATURATED								
3.5	2.5	1.0	2.694	1.023	1.028	2.63	188	71
5.0	2.5	2.5	2.745	1.030	1.034	2.66	182	68
7.5	2.5	5.0	2.818	1.043	1.043	2.70	157	63
10.0	2.5	7.5	2.868	1.061	1.053	2.71	157	52
12.5	2.5	10.0	2.894	1.080	1.068	2.69	157	48
17.5	2.5	15.0	2.960	1.106	1.098	2.69	134	44

COMMENT: Shear wave polarization randomly oriented.
Poor signal at lowest confining pressure level.

Table 51

Ultrasonic compressional and shear wave velocities and associated seismic attenuations for dry and water saturated conditions as a function of confining pressure

SAMPLE ID:	G4-1617.75-SNL-A-1
ORIENTATION:	VERTICAL
PORE FLUID:	DRY/WATER
TEMPERATURE, ° C:	22
SAMPLE LENGTH, mm:	25.68
SAMPLE DIAMETER, mm:	23.95
VACUUM DRY WEIGHT, g:	18.666
ROOM DRY WEIGHT, g:	18.979
SAT WEIGHT, g:	22.031
DRY BULK DENSITY, g/cm^3:	1.613
POROSITY, %:	29.1

PRESSURE (MPa)			VELOCITY (km/s^{-1})			VP/VS	1000/Q	
CONF	PORE	DIFF	P-WAVE	S1-WAVE	S2-WAVE	RATIO	P-WAVE	S2-WAVE
ROOM DRY								
1.0	0.0	1.0	2.927	2.019	1.959	1.47	155	149
2.5	0.0	2.5	3.139	2.061	1.974	1.56	155	149
5.0	0.0	5.0	3.142	2.000	2.008	1.57	155	149
7.5	0.0	7.5	3.142	2.016	2.027	1.55	154	149
10.0	0.0	10.0	3.146	2.025	2.043	1.55	154	149
15.0	0.0	15.0	3.154	2.045	2.046	1.54	155	149
SATURATED								
3.5	2.5	1.0	3.382	1.759	1.760	1.92	180	44
5.0	2.5	2.5	3.391	1.764	1.765	1.92	180	44
7.5	2.5	5.0	3.409	1.781	1.782	1.91	180	44
10.0	2.5	7.5	3.409	1.793	1.795	1.90	137	40
12.5	2.5	10.0	3.428	1.814	1.812	1.89	137	40
17.5	2.5	15.0	3.437	1.824	1.823	1.88	125	40

COMMENT: Shear wave polarization randomly oriented.

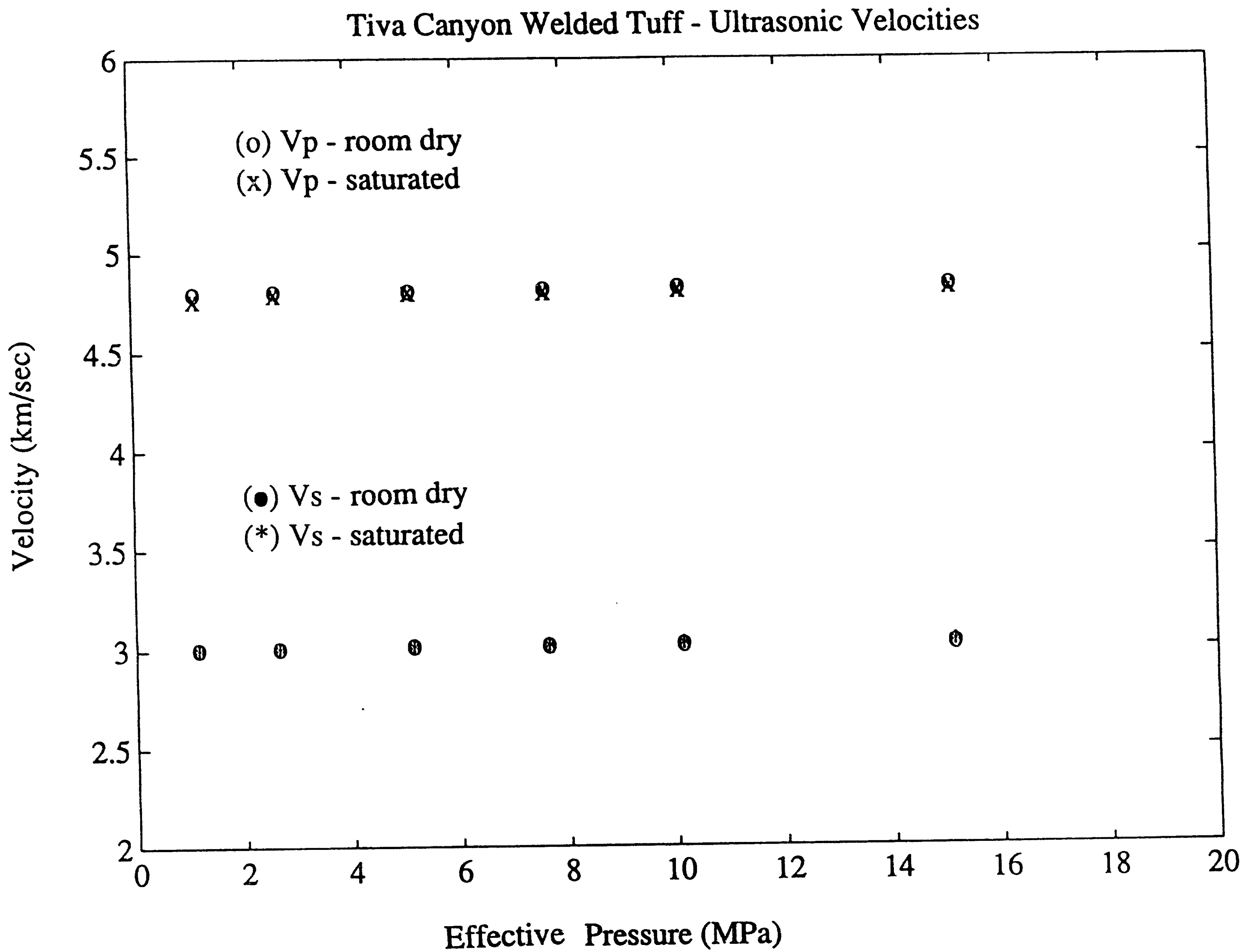

Figure 11a: The compressional and shear wave velocities for dry and saturated conditions are shown as a function of pressure for a Tiva Canyon tuff (GU3-211.3-SNL-A2). The solid symbols indicate data collected in a saturated condition; the open symbols indicate data collected in a dry condition. Circles are compressional velocity; the squares are shear wave data.

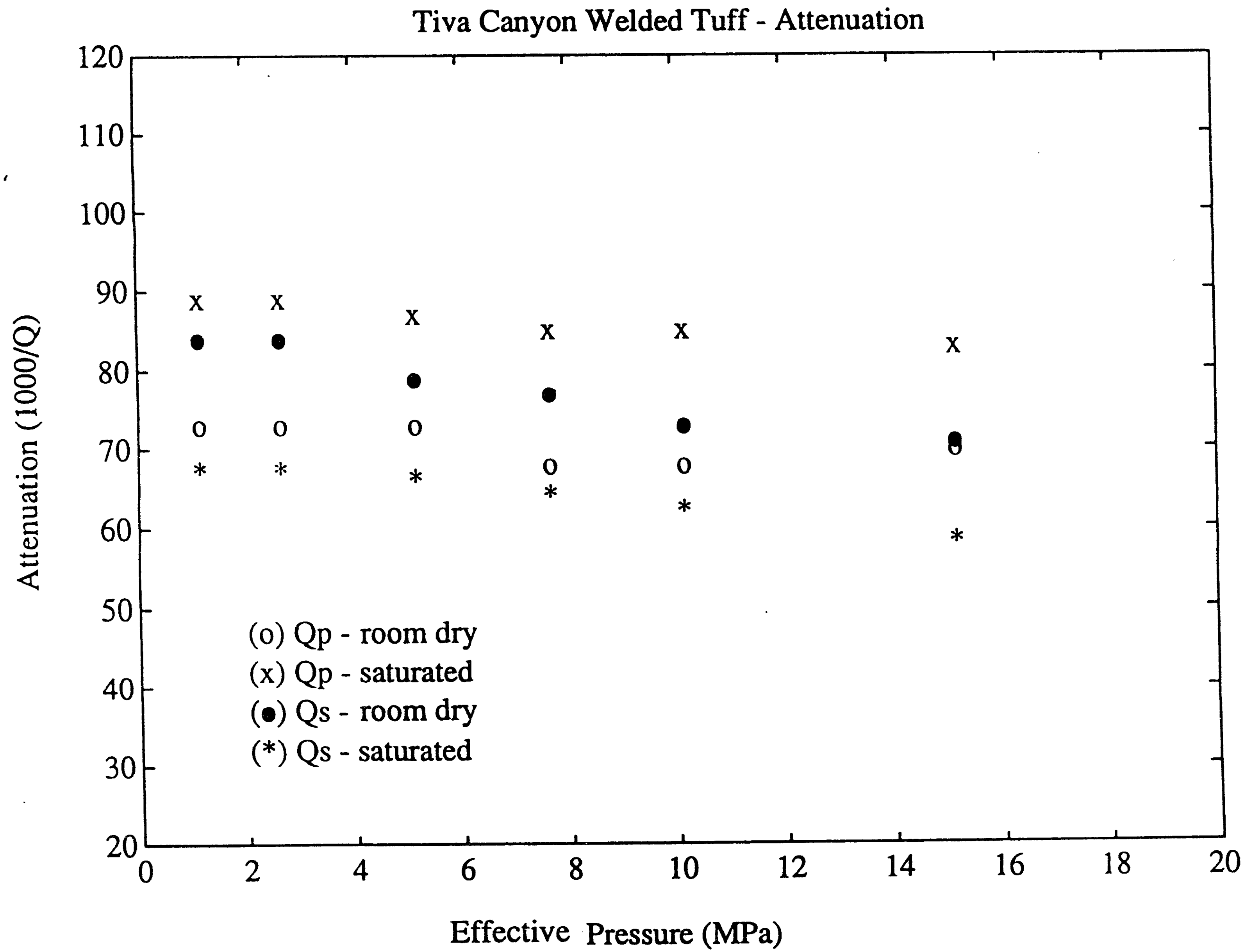

Figure 11b: The seismic wave attenuation is shown as a function of confining pressure for a specimen of Tiva Canyon tuff (GU3-211.3-SNL-A2). The solid symbols are attenuation measured in the saturated state; the open symbols indicate data collected on a dry specimen. Circles indicate compressional attenuation; squares indicate shear attenuation.

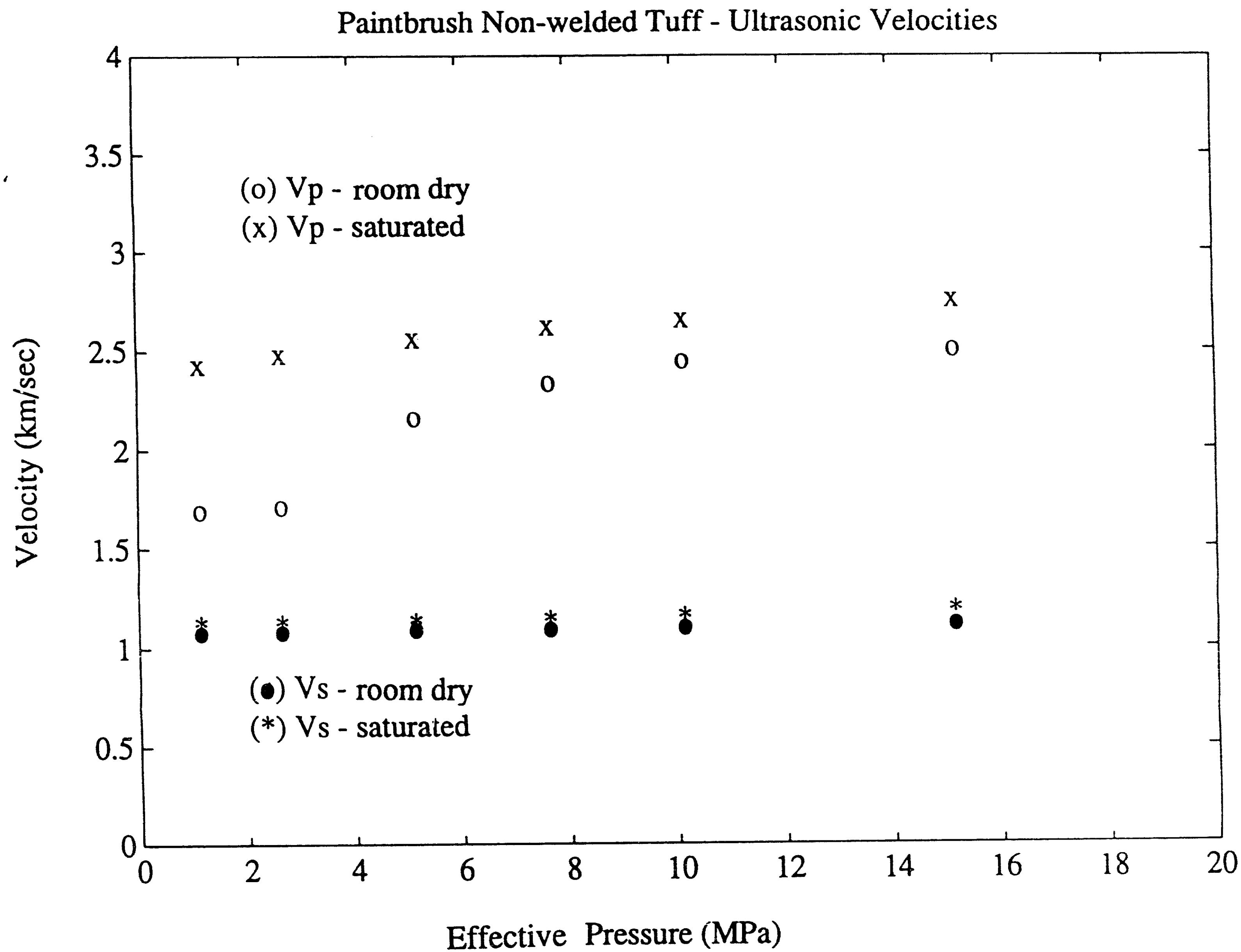

Figure 12a: Compressional and shear wave velocities for a specimen of the Paintbrush tuff (G2-7097-SNL-B) are shown as a function of confining pressure. The solid symbols indicate data collected under saturated conditions; the open circles indicate data collected in a dry state. Circles are compressional velocity; the squares indicate shear velocity.

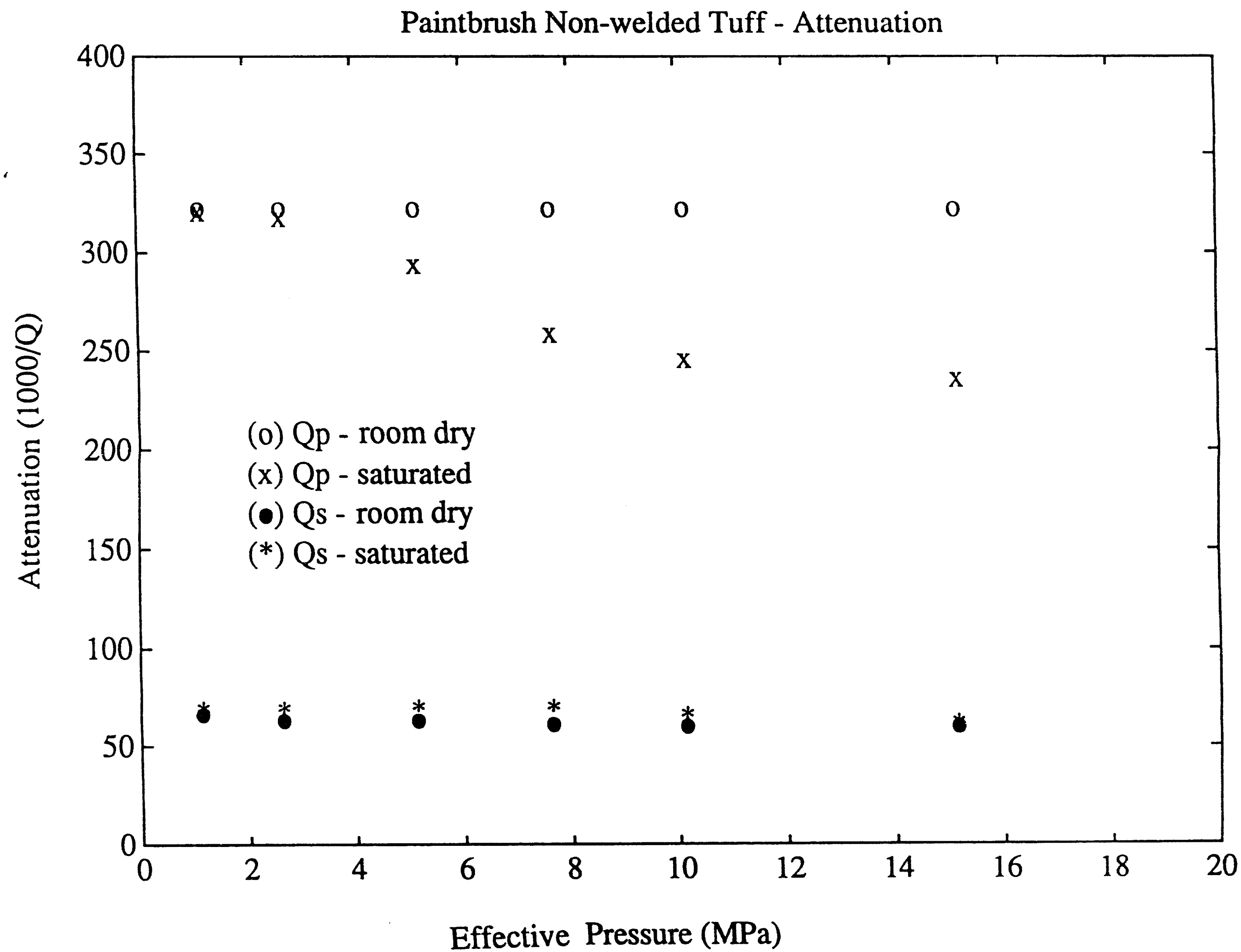

Figure 12b: Seismic wave attenuation is plotted as a function of confining pressure for a specimen of the Paintbrush tuff (G2-709.7-SNL-B). The solid symbol indicates data collected under saturated conditions; the open symbol indicates data collected for a dry state. Circles indicate compression attenuation; squares represent shear attenuation.

4.0 DISCUSSION

Four techniques were used to measure Young's modulus and Q^{-1} as a function of frequency, strain amplitude, and saturation for specimens of the tuff from near and on Yucca Mountain. Dispersion data for Young's modulus and extensional attenuation were obtained for one specimen of Topopah Spring Member (TSw2) tuff. The different techniques produced comparable results. Differences observed in the attenuation values obtained using the waveform inversion and resonant bar techniques are attributable to sample inhomogeneity. Tuff is highly heterogeneous, yielding a large scatter in rock properties (e.g. Price et al., 1987). The inhomogeneities in the tuff (e.g., pores, pumice fragments, vapor phase altered zones, lithics, and lithophysae) range in size from microscopic to several centimeters. The relatively small subsamples taken for these measurements probably contain different quantities of inhomogeneities, producing scatter in the modulus and attenuation data for the two techniques. Comparisons of these techniques on relatively homogeneous granite specimens with uniform grain sizes on the order of 0.5 mm, yield nearly identical moduli and attenuations for dry specimens (Haupt et al., 1992).

The partial data sets obtained for the other tuff specimens were not sufficient to define the modulus dispersion. However, these results are useful for examining the relative differences in modulus and attenuation caused by porosity, fabric, sample heterogeneity, and compositional variations.

4.1 Young's Modulus: The Effects of Frequency and Water Saturation

Young's modulus shows a slight frequency dependence in room dry tuff. The moduli for the saturated tuff typically are less than the corresponding room dry measurements, except at ultrasonic frequencies, at which the data are inconsistent. The reduction in modulus for the saturated state can be attributed to the reduction of surface energy along the grain boundaries, microcracks, and pores within the rock (Murphy, 1982; Bulau et al., 1984; Murphy et al., 1984). Modulus reduction is more pronounced in granite and other low porosity crystalline rocks than for the tuff. This is due, at least in part, to the pore geometry. Granites are characterized by low aspect ratio cracks, whereas the pore structure of the welded tuff consists predominantly of ellipsoidal pores and lithophysal zones (Price et al., 1987).

The frequency dependence of the modulus can be attributed to fluid flow within the sample. When the cyclic loading rate exceeds the time constant for fluid diffusion within the pore space, the specimen begins to stiffen because of the compression of the pore water. In turn, the *effective* modulus increases. The point at which the relative stiffening occurs is directly related to the sample diameter, the pore geometry, and the boundary conditions for fluid flow within the specimen (Spencer, 1981; Dunn, 1987).

4.2 Attenuation: The Effects of Frequency and Water Saturation

The Q_E^{-1} in the room dry condition is relatively low and is, at least to the first order, independent of frequency. These observations are consistent with previous data (Spencer, 1981; Winkler et al., 1979; Murphy et al., 1984). The resonant bar and waveform inversion data exhibit a significant difference in Q_E^{-1} that is attributable to sample heterogeneity. Lucet et al. (1991) have shown that sample heterogeneity significantly affects the modulus and attenuation measurements.

Water-saturated welded tuffs show larger Q_E^{-1} than the room dry specimens at nearly all frequencies. The attenuation is frequency dependent. At frequencies less than 1 Hz, the dry and saturated attenuation for tuff are nearly the same. However, at higher frequencies (between 1 and 10^2 Hz), Q_E^{-1} increases nearly fivefold. Between 10^4 and 2×10^5 Hz, resonant bar and waveform inversion techniques display a consistently greater attenuation for the saturated condition than for the dry condition. Comparisons between the measurements at these frequencies do not yield consistent results; the differences are most likely caused by sample heterogeneity.

The increase in Q_E^{-1} with frequency for water-saturated specimens can be attributed to a number of mechanisms. The fluid flow in the pores is strongly frequency-dependent and can give rise to attenuation. Models have been proposed by Gardner (1962), Walsh (1969), Mavko and Nur (1979), O'Connell and Budiansky (1977), and White (1986) to explain the experimental data; attenuation is attributed to the relative motion between the fluid and pore. As the loading frequency increases, the rate of fluid flow increases and viscous losses control the attenuation. Once the deformation rate is significantly greater than the pore fluid response, stiffening occurs and attenuation decreases. The data for tuff does not exhibit the stiffening or the corresponding decrease in attenuation. Fluid flow is governed by the boundary conditions imposed by the experimental setup, the sample geometry, and the pore geometry. For the small diameter tuff specimens with a relatively high porosity and rounded pores, flow in and out of the pores and stiffening of the fluid was minimal.

(Note: All the specimens were tested under drained conditions.)

4.3 Effect of Strain Amplitude on Modulus and Attenuation

The effect of strain amplitude on Young's modulus and seismic wave attenuation has been considered by a number of investigators (Walsh, 1969; Mavko, 1979; Winkler et al., 1979). For rocks with low aspect ratio cracks, the modulus has been shown to decrease with increasing strain amplitude. Several models have been forwarded to explain the decrease. Walsh (1969), Mavko (1979), and Winkler et al. (1979) have proposed frictional mechanisms in which sliding on microcracks dissipates energy, observed as attenuation. Alternative mechanisms based on changes in surface energy and movement of fluid films in partially saturated rocks have been proposed by Spencer (1981), Mavko and Nur (1979), Bulau et al. (1984) and Murphy et al. (1984). Young's modulus and attenuation for the tuff showed no strain amplitude dependence for either the dry or saturated conditions. By way of comparison, the attenuation in granite increases markedly as the strain amplitude is increased from 5×10^{-7} to 5×10^{-4} (Haupt et al., 1992). The transition to frequency-dependent attenuation occurs at strain amplitudes approaching 10^{-5} for dry granite and 10^{-6} for saturated granite. The frequency shift observed for the granite is most likely related to flow within the pores. The absence of any strain amplitude dependence in the saturated specimens of the tuff is probably because the time constant for diffusion is short for the pore geometry in the tuff and the experimental boundary conditions.

5.0 CONCLUSIONS

The effects of frequency and water saturation on Young's modulus and on attenuation for selected samples of the Paintbrush Tuff formation on and near Yucca Mountain have been studied. The experiments were conducted at room temperature and pressure using a variety of techniques to span the frequency range from 10^{-2} to 10^{6} Hz. The data indicate that frequency has a limited effect on the modulus as well as on the attenuation over the entire frequency range. A small frequency dependence was observed for saturated samples. The effects of pressure and strain amplitude on modulus and attenuation were also very small at least for welded tuff. (In this context, *small* is used in comparison to what is normally observed in crystalline rocks with low aspect ratio cracks.) The results of these measurements are consistent with theoretical models that have been developed. Since the tuff is composed primarily of ellipsoidal and spherical pores, small pressure and strain amplitude dependencies were anticipated. The effect of saturation is to reduce Young's modulus by several percent in most instances. Water saturation also tended to increase the attenuation at each frequency.

The measurements of seismic wave velocity, Young's modulus, and attenuation reported are important, not only to constrain the microstructure of the tuff but also important in correlating laboratory scale properties with field measurements. At least two types of seismic surveys have been carried out at Yucca Mountain; surface seismic and vertical seismic profiling. The acoustic and mechanical data in this study can be used to constrain the seismic sections. We have shown that the modulus is independent of frequency at least for dry specimens. Since many of the rocks of interest are above the water table the velocity data collected, particularly on the dry specimens can be directly applied to the data.

The velocity and attenuation data for dry and saturated conditions at low frequencies (less than 100 Hz) can be incorporated into seismic response models. The data is relevant to calculations of the seismic response due to earthquake loading at the potential repository. These models are extremely important in predicting the response of rock units to seismic (earthquake) forcing.

6.0 REFERENCES

Bulau, J. R., B. R. Tittmann, M. Abdel-Gawad, and C. Salvado, 1984, The Role of Aqueous Fluids in the Internal Friction of Rock: J. Geophys. Res. 89(B6), 4207-4212. (NNA.930215.0042)

Coyner, Karl B., 1984, Effects of Stress, Pore Pressure, and Pore Fluids on Bulk Strain, Velocity, and Peremeability in Rocks: Ph.D. Thesis, Massachusetts Institute of Technology. (NNA.930330.0062)

Dunn, K. J., 1986, Acoustic Attenuation in Fluid-Saturated Porous Cylinders at Low Frequencies: J. Acoustic Soc. Am. 79(6), 1709-1721. (NNA.920218.0003)

Dunn, K. J., 1987, Sample Boundary Effect in Acoustic Attenuation of Fluid-Saturated Porous Cylinders: J. Acoustic Soc. Am. 81(5), 1259-1266. (NNA.920218.0004)

Gardner, G. H. F., 1962, Extensional Waves in Fluid-Saturated Porous Cylinders: J. Acoustic Soc.Am. 34(1), 36-40.(NNA.920218.0005)

Gordon, R. B., and L. A. Davis, 1968, Velocity and Attenuation of Seismic Waves in Imperfectly Elastic Rock: J. Geophys. Res. 73, 3917-3935.(NNA.920218.0007)

Haupt, R. W., R. J. Martin, X. Tang, W. Dupree, and R. H. Price, 1992"Modulus Dispersion and Attenuation in Tuff and Granite", Proc. 33rd U.S. Symposium on Rock Mechanics, Tillerson and Wawersik, W. (ed),899-908.(NNA.930824.0002)

Lucet, N., P. N. Rasolofosaon, and B. Zinsner, 1991, Sonic Properties of Rocks Under Confining Pressure Using the Resonant Bar Technique: J. Acoustic Soc. Am. 89(3), 980-990.(NNA.920225.0038)

Mavko, G. M., 1979, Frictional Attenuation: An Inherent Amplitude Dependence: J. Geophys. Res. 84, 4769-4775.(NNA.920218.0008)

Mavko, G. and A. Nur, 1979, Wave Attenuation in Partially Saturated Rocks: Geophysics 44, 161-178.(NNA.920218.0009)

Murphy, W. F., III, 1982, Effects of Partial Water Saturation on Attenuation in Massillon Sandstone and Vycor Porous Glass: J. Acoustic Soc. Am. 71(6), 1458-1468. (NNA.930224.0138)

Murphy, W. F., III, K.W. Winkler and R.L. Kleinberg, 1984, Frame Modulus Reduction in Sedimentary Rocks: The Effect of Adsorption on Grain Contacts: J. Geophys. Res. Lett., 9, 805-808. (NNA.920218.0010)

O'Connell, R. J. and B. Budiansky, 1977, Viscoelastic Properties of Fluid-Saturated Cracked Solids: J. Geophys. Res. 82, 5719-5735. (NNA.920218.0012)

Oritz, T. S., R. L. Williams, F. B. Nimick, B. C. Whittet, and D. L, South, 1985, A Three Dimensional Model of Reference Thermal/mechanical and Hydrologic Stratigraphy at Yucca Mountain, Southern Nevada: SAND84-1076, Sandia National Laboratories Albuquerque, NM. (NNA.890315.0013)

Paffenholz, J. and H. Burkhardt, 1989, Absorption and Modulus Measurements in the Seismic Frequency and Strain Range on Partially Saturated Sedimentary Rocks: J. Geophys. Res. 94, 9493-9507. (NNA.920218.0013)

Price, R. H., J. R. Connolly, and K. Keil, 1987, Petrologic and Mechanical Properties of Outcrop Samples of the Welded, Devitified Topopah Spring Member of the Paintbrush Tuff: Sandia Report, SAND86-1131 UC-70. (HQS.880517.1704)

Spencer, J. W., 1981, Stress Relaxations at Low Frequencies in Fluid-Saturated Rocks: Attenuation and Modulus Dispersion: J. Geophys. Res. 86, 1803-1812. (NNA.920218.0015)

Tang, X., 1992, A Waveform Inversion Technique for Measuring Elastic Wave Attenuation in Cylindrical Bars: Geophys. 57, 854-859. (NNA.921112.0081)

Tittmann, B. R., V. A. Clark, J.M. Richardson, and T.W. Spencer, 1980, Possible Mechanism for Seismic Wave Attenuation in Rocks Containing Small Amounts of Volatiles, J. Geophys. Res., 85, 5199-5208. (NNA.930215.0043)

Toksöz, M. N., D. H. Johnston, and A.Timur, 1979, Attenuation of Seismic Waves in Dry and Saturated Rocks: I. Laboratory Measurements: Geophys. 44, 681-690. (NNA.920218.0016)

Toksöz, M. N., and D. H. Johnston, 1981, Seismic Wave Attenuation: Geophys. reprint series, No.2. (NNA.930414.0034)

Toksöz, M. N., B. Mandal, and A. M. Dainty, 1990, Frequency Dependent Attenuation in the Crust, Geophys. Res. Lett., 17, 973-976. (NNA.931012.0003)

Walsh, J. B., 1969, Seismic Wave Attenuation in Rock Due to Friction: J. Geophys. Res. 71, 2591-2599. (NNA.930215.0044)

White, E. J., 1986, Biot-Gardner Theory of Extensional Waves in Porous Rocks: Geophysics, 51, 742-745. (NNA.920218.0017)

Winkler, D., A. Nur, and M. Gladwin, 1979, Friction and Seismic Attenuation in Rocks Nature 277, 528-531. (NNA.920218.0018)

Appendix

Information from the Reference Information Base
Used in this Report

This report contains no information from the Reference Information Base.

Candidate Information
for the
Reference Information Base

This report contains no candidate information fro the Reference Information Base.

Candidate Information
for the
Geographic Nodal Information Study
and Evaluation System

This report contains no candidate information for the Geographic Nodal Information Study and Evaluation System.

YUCCA MOUNTAIN SITE CHARACTERIZATION PROJECT

DISTRIBUTION LIST

1 D.A. Dreyfus (RW-1)
Director
OCRWM
US Department of Energy
1000 Independence Avenue SW
Washington, DC 20585

1 L.H. Barrett (RW-2)
Acting Deputy Director
OCRWM
US Department of Energy
1000 Independence Avenue SW
Washington, DC 20585

1 J.D. Saltzman (RW-4)
Office of Strategic Planning and International Programs
OCRWM
US Department of Energy
1000 Independence Avenue SW
Washington, DC 20585

1 J.D. Saltzman (RW-5)
Office of External Relations
OCRWM
US Department of Energy
1000 Independence Avenue SW
Washington, DC 20585

1 Samuel Rousso (RW-10)
Office of Program and Resource Mgt.
OCRWM
US Department of Energy
1000 Independence Avenue SW
Washington, DC 20585

1 J. C. Bresee (RW-10)
OCRWM
US Department of Energy
1000 Independence Avenue SW
Washington, DC 20585

1 R.M. Nelson (RW-20)
Office of Geologic Disposal
OCRWM
US Department of Energy
1000 Independence Avenue, SW
Washington, DC 20585

1 S. J. Brocoum (RW-22)
Analysis and Verification Division
OCRWM
US Department of Energy
1000 Independence Avenue SW
Washington, DC 2585

1 D. Shelor (RW-30)
Office of Systems and Compliance
OCRWM
US Department of Energy
1000 Independence Avenue, SW
Washington, DC 20585

1 J. Roberts (RW-33)
Director, Regulatory Compliance Division
OCRWM
US Department of Energy
1000 Independence Avenue, SW
Washington, DC 20585

1 G. J. Parker (RW-332)
Reg. Policy/Requirements Branch
OCRWM
US Department of Energy
1000 Independence Avenue, SW
Washington, DC 20585

1 R. A. Milner (RW-40)
Office of Storage and Transporation
OCRWM
US Department of Energy
1000 Independence Avenue, SW
Washington, DC 20585

1 S. Rousso (RW-50)
Office of Contract Business Management
OCRWM
US Department of Energy
1000 Independence Avenue, SW
Washington, DC 20585

1 T. Wood (RW-52)
Director, M&O Management Division
OCRWM
US Department of Energy
1000 Independence Avenue, SW
Washington, DC 20585

4 Victoria F. Reich, Librarian
Nuclear Waste Technical Review Board
1100 Wilson Blvd, Suite 910
Arlington, VA 22209

5 R.M. Nelson Jr, Acting Project Manager
Yucca Mountain Site Characterization Office
US Department of Energy
P.O. Box 98608--MS 523
Las Vegas, NV 89193-8608

1 C. L. West, Director
Office of External Affairs
DOE Nevada Field Office
US Department of Energy
P.O. Box 98518
Las Vegas, NV 89193-8518

8 Technical Information Officer
DOE Nevada Field Office
US Department of Energy
P.O. Box 98518
Las Vegas, NV 89193-8518

1 P. K. Fitzsimmons, Technical Advisor
Office of Assistant Manager for Environmental Safety and Health
DOE Nevada Field Office
US Department of Energy
P.O. Box 98518
Las Vegas, NV 89193-8518

1 D. R. Elle, Director
Environmental Protection and Division
DOE Nevada Field Office
US Department of Energy
P.O. Box 98518
Las Vegas, NV 89193-8518

1 Repository Licensing & Quality Assurance
Project Directorate
Division of Waste Management
US NRC
Washington, DC 20555

1 Senior Project Manager for Yucca Mountain
Repository Project Branch
Division of Waste Management
US NRC
Washington, DC 20555

1 NRC Document Control Desk
Division of Waste Management
US NRC
Washington, DC 20555

1 Philip S. Justus
NRC Site Representive
301 E Stewart Avenue, Room 203
Las Vegas, NV 89101

1 E. P. Binnall
Field Systems Group Leader
Building 50B/4235
Lawrence Berkeley Laboratory
Berkeley, CA 94720

1 Center for Nuclear Waste Regulatory Analyses
6220 Culebra Road
Drawer 28510
San Antonio, TX 78284

3 W. L. Clarke
Technical Project Officer - YMP
Attn: YMP/LRC
Lawrence Livermore National Laboratory
P.O. Box 5514
Livermore, CA 94551

1 J. A. Blink
Deputy Project Leader
Lawrence Livermore National
Laboratory
101 Convention Center Drive
Suite 820, MS 527
Las Vegas, NV 89109

4 J. A. Canepa
Technical Project Officer - YMP
N-5, Mail Stop J521
Los Alamos National Laboratory
P.O. Box 1663
Los Alamos, NM 87545

1 H. N. Kalia
Exploratory Shaft Test Manager
Los Alamos National Laboratory
Mail Stop 527
101 Convention Center Dr., #820
Las Vegas, NV 89101

1 N. Z. Elkins
Deputy Technical Project Officer
Los Alamos National Laboratory
Mail Stop 527
101 Convention Center Dr., #820
Las Vegas, NV 89101

5 L. E. Shephard
Technical Project Officer - YMP
Sandia National Laboratories
Organization 6302, M/S 1333
P.O. Box 5800
Albuquerque, NM 87185

1 J. F. Devine
Asst Director of Engineering Geology
US Geological Survey
106 National Center
12201 Sunrise Valley Drive
Reston, VA 22092

1 L. R. Hayes
Technical Project Officer
Yucca Mountain Project Branch
MS 425
US Geological Survey
P.O. Box 25046
Denver, CO 80225

1 V. R. Schneider
Asst. Chief Hydrologist--MS 414
Office of Program Coordination
and Technical Support
US Geological Survey
12201 Sunrise Valley Drive
Reston, VA 22092

1 J. S. Stuckless
Geologic Division Coordinator
MS 913
Yucca Mountain Project
US Geological Survey
P.O. Box 25046
Denver, CO 80225

1 D. H. Appel, Chief
Hydrologic Investigations Program
MS 421
US Geological Survey
P.O. Box 25046
Denver, CO 80225

1 E. J. Helley
Branch of Western Regional Geology
MS 427
US Geological Survey
345 Middlefield Road
Menlo Park, CA 94025

1 R. W. Craig, Chief
Nevada Operations Office
US Geological Survey
101 Convention Center Drive
Suite 860, MS 509
Las Vegas, NV 89109

1 D. Zesiger
US Geological Survey
101 Conventional Center Drive
Suite 860, MS 509
Las Vegas, NV 89109

1 G. L. Ducret, Associate Chief
Yucca Mountain Project Division
US Geological Survey
P.O. Box 25046
421 Federal Center
Denver, CO 80225

1 **A. L. Flint**
US Geological Survey
MS 721
P.O. Box 327
Mercury, NV 89023

1 **D. A. Beck**
Water Resources Division, USGS
6770 S Paradise Road
Las Vegas, NV 89119

1 **P. A. Glancy**
US Geological Survey
Federal Building, Room 224
Carson City, NV 89701

1 **Sherman S.C. Wu**
US Geological Survey
2255 N. Gemini Drive
Flagstaff, AZ 86001

1 **J. H. Sass - USGS**
Branch of Tectonophysics
2255 N Gemini Drive
Flagstaff, AZ 86001

1 **DeWayne Campbell**
Technical Project Officer - YMP
US Bureau of Reclamation
Code D-3790
P.O. Box 25007
Denver, CO 80225

1 **J. M. LaMonaca**
Records Specialist
US Geological Survey
421 Federal Center
P.O. Box 25046
Denver, CO 80225

1 **W. R. Keefer - USGS**
913 Federal Center
P.O. Box 25046
Denver, CO 80225

1 **M. D. Voegele**
Technical Project Officer - YMP
SAIC
101 Convention Center Drive
Suite 407
Las Vegas, NV 89109

2 **L. D. Foust**
Nevada Site Manager
TRW Environmental Safety Systems
101 Convention Center Drive
Suite 540, MS 423
Las Vegas, NV 89109

1 **C. E. Ezra**
YMP Support Office Manager
EG&G Energy Measurements Inc
MS V-02
P.O. Box 1912
Las Vegas, NV 89125

1 **Jan Docka**
Roy F. Weston Inc
955 L'Enfant Plaza SW
Washington, DC 20024

1 **Technical Information Center**
Roy F. Weston Inc
955 L'Enfant Plaza SW
Washington, DC 20024

1 **D. Hedges, Vice President, QA**
Roy F. Weston Inc
4425 Spring Mountain Road
Suite 300
Las Vegas, NV 89102

1 **D. L. Fraser, General Manager**
Reynolds Electrical & Engineering Co, Inc
MS 555
P.O. Box 98521
Las Vegas, NV 89193-8521

1 **B. W. Colston, President and General Manager**
Las Vegas Branch
Raytheon Services Nevada
MS 416
P.O. Box 95487
Las Vegas, NV 89193-5487

1 **R. L. Bullock**
Technical Project Officer - YMP
Raytheon Services Nevada
Suite P-250, MS 403
101 Convention Center Drive
Las Vegas, NV 89109

1 Paul Eslinger, Manager
PASS Program
Pacific Northwest Laboratories
P.O. Box 999
Richland, WA 99352

1 A. T. Tamura
Science and Technology Division
OSTI
US Department of Energy
P.O. Box 62
Oak Ridge, TN 37831

1 Carlos G. Bell Jr
Professor of Civil Engineering
Civil and Mechanical Engineering Dept.
University of Nevada, Las Vegas
4505 S Maryland Parkway
Las Vegas, NV 89154

1 P. J. Weeden, Acting Director
Nuclear Radiation Assessment Div.
US EPA
Environmental Monitoring
Systems Lab
P.O. Box 93478
Las Vegas, NV 89193-3478

1 ONWI Library
Battelle Columbus Laboratory
Office of Nuclear Waste Isolation
505 King Avenue
Columbus, OH 43201

1 T. Hay, Executive Assistant
Office of the Governor
State of Nevada
Capitol Complex
Carson City, NV 89710

3 R. R. Loux
Executive Director
Agency for Nuclear Projects
State of Nevada
Evergreen Center, Suite 252
1802 N. Carson Street
Carson City, NV 89710

1 C.H. Johnson
Technical Program Manager
Agency for Nuclear Projects
State of Nevada
Evergreen Center, Suite 252
1802 N. Carson Street
Carson City, NV 89710

1 John Fordham
Water Resources Center
Desert Research Institute
P.O. Box 60220
Reno, NV 89506

1 David Rhode
Desert Research Institute
P.O. Box 60220
Reno, NV 89506

1 Eric Anderson
Mountain West Research-
Southwest Inc
2901 N Central Avenue #1000
Phoenix, AZ 85012-2730

1 The Honorable Cyril Schank
Chairman
Churchill County Board of
Commissioners
190 W First Street
Fallon, NV 89406

1 Dennis Bechtel, Coordinator
Nuclear Waste Division
Clark County Department of
Comprehensive Planning
301 E Clark Avenue, Suite 570
Las Vegas, NV 89101

1 Juanita D. Hoffman
Nuclear Waste Repository
Oversight Program
Esmeralda County
P.O. Box 490
Goldfield, NV 89013

1 Eureka County Board of Commissioners
Yucca Mountain Information
Office
P.O. Box 714
Eureka, NV 89316

1 Brad Mettam
Inyo County Yucca Mountain
Repository Assessment Office
Drawer L
Independence, CA 93526

1 Lander County Board of
Commissioners
315 South Humbolt
Battle Mountain, NV 89820

1 Vernon E. Poe
Office of Nuclear Projects
Mineral County
P.O. Box 1026
Hawthorne, NV 89415

1 Les W. Bradshaw
Program Manager
Nye County Nuclear Waste
Repository Program
P.O. Box 153
Tonopah, NV 89049

1 Florindo Mariani
White Pine County Nuclear
Waste Project Office
457 Fifth Street
Ely, NV 89301

1 Judy Foremaster
City of Caliente Nuclear Waste
Project Office
P.O. Box 158
Caliente, NV 89008

1 Phillip A. Niedzielski-Eichner
Nye County Nuclear Waste
Repository Project Office
P.O. Box 221274
Chantilly, VA 22022-1274

1 Jason Pitts
Lincoln County Nuclear Waste
Project Office
Lincoln County Courthouse
Pioche, NV 89043

1 Economic Development Dept.
City of Las Vegas
400 E. Stewart Avenue
Las Vegas, NV 89101

1 Commmunity Planning and
Development
City of North Las Vegas
P.O. Box 4086
North Las Vegas, NV 89030

1 Community Development and
Planning
City of Boulder City
P.O. Box 61350
Boulder City, NV 89006

1 Commission of the European
Communities
200 Rue de la Loi
B-1049 Brussells
BELGIUM

2 M. J. Dorsey, Librarian
YMP Research and Study Center
Reynolds Electrical &
Engineering Co Inc
MS 407
P.O. Box 98521
Las Vegas, NV 89193-8521

1 Amy Anderson
Argonne National Laboratory
Building 362
9700 S Cass Avenue
Argonne, IL 60439

1 Steve Bradhurst
P.O. Box 1510
Reno, NV 89505

1 Michael L. Baughman
35 Clark Road
Fiskdale, MA 01518

1 Glenn Van Roekel
Director of Community
Development
City of Caliente
P.O. Box 158
Caliente, NV 89008

1 Ray Williams, Jr
P.O. Box 10
Austin, NV 89310

1 Nye County District Attorney
P.O. Box 593
Tonopah, NV 89049

1 William Offutt
Nye County Manager
Tonopah, NV 89049

1 Charles Thistlethwaite, AICP
Associate Planner
Inyo County Planning Department
Drawer L
Independence, CA 93526

1 R. F. Pritchett
Technical Project Officer - YMP
Reynolds Electrical &
Engineering Company Inc
MS 408
P.O. Box 98521
Las Vegas, NV 89193-8521

1 Dr. Moses Karakouzian
1751 E Reno #125
Las Vegas, NV 89119

10 R.J. Martin III
New England Research Inc
76 Olcott Drive
White River Junction, VT 05001

	MS	
1	1325	L.S. Costin, 6313
2	1330	G.M. Gerstner-Miller, 6352 100/1232713/SAND92-0847/QA
2	1330	G.M. Gerstner-Miller, 6352 DRMS Files
20	1330	WMT Library, 6352
1	1324	P.B. Davies, 6115
1	0827	P.J. Hommert, 1502
1	1375	D.A. Dahlgren, 4400
20	1325	R.H. Price, 6313
1	0751	W.R. Wawersik, 6117
5	0899	Technical Library, 13414
1	0619	Technical Publications, 13416
10	0100	Document Processing for DOE/OSTI, 7613-2
1	9018	Central Technical Files, 8523-2

DATE
FILMED
9/19/94

END